Design and characterisation of a continuous rotary damper with ideal viscous damping properties

Loh Wenhao
B.Eng. (Hons.), NUS

A THESIS SUBMITTED

FOR THE DEGREE OF MASTER OF ENGINEERING

DEPARTMENT OF MECHANICAL ENGINEERING

NATIONAL UNIVERSITY OF SINGAPORE

2012

Declaration

I hereby declare that this thesis is my original work and it has been written by me in its entirety. I have duly acknowledged all the sources of information which have been used in the thesis.

This thesis has also not been submitted for any degree in any university previously.

Loh Wenhao

15th November 2012

Acknowledgements

I would like to express my deepest appreciation to my supervisor, Assoc. Prof Chew Chee Meng for his patience and guidance during this project. If not for Prof Chew and his invention of the Series Damper Actuator, this dissertation would certainly not have been possible. I would also like to thank my co-supervisor, Dr Lim Chee Wang of Singapore Institute of Manufacturing Technology, for supporting this project and for offering timely advice when I encountered numerous problems.

I would like extend my thanks to my colleagues, Shen Bing Quan and Li Renjun for their support and help. I would also like to thank all the laboratory assistants of Control Lab 1 and 2 for their unyielding patience, and assistance in finding the necessary equipment for my experiments.

Finally, I would like to express my deepest gratitude to my family and my fiancé, who supported me throughout the duration of this project mentally, spiritually and financially.

Abstract

This thesis has presented work done to design a continuous rotary damper with ideal viscous damping properties for use in the implementation of the Series Damper Actuator (SDA).

An extensive study is done into the designs of existing commercial dampers, as well as various other prototypes developed by independent groups. The first prototype continuous rotary damper was designed based on existing limited angle viscous dampers, and builds on the work done by Chang [1] in 2005. The new design overcame the mechanical challenges that Chang met, and a functioning prototype was fabricated.

The first damper was tested and characterised by Alt [2] in 2012, during which several new flaws were noted. A new damper, based on the concept of a radial piston pump, was designed to overcome the flaws of the first damper. A functioning prototype was fabricated, and subsequently tested and characterised.

This thesis focuses on the design process taken to develop both dampers, and lists the major considerations taken at every stage to improve the performance of the damper. In addition to the analysis of the behaviour of the damper output, several suggestions were made that could be taken up by future research.

Table of Contents

List of Tables

List of Figures

Chapter 1 - Introduction

1.1 Background

In recent decades, the field of robotics has advanced greatly and has been increasingly applied to many fields. It has been most successful in the implementation of position and velocity control of each degree of freedom [3-6]. In closed known environments, such robots perform well, and are able to execute repetitive tasks with speed and accuracy. Examples of such task are simple pick and place operations, automatic welding, CNC machining, et cetera.

However, in situations where interactions with an unknown environment are required, such as grasping objects of unknown irregular shapes, maintaining constant contact with a work piece in de-burring machining processes, traditional position and velocity do not perform as well. In these situations, force control is required [7, 8]. Successful force control has two aspects. One is use algorithm and sensor information to achieve a desired force at the end-effector by controlling the force output of the individual actuators in the robot [9-11]. The other is generating some desired torque at the actuator itself [10-13].

Actuation technology had been typically poor at generating and sustaining an accurate output force. It was also poor at holding a poor output impedance [14]. Force control was largely achieved by locating a force sensor at the end-effector and implementing a feedback loop without directly controlling the force output of the individual actuators [15-18].

With the advent of the force control actuation concept, some headway has been made into its research. Several systems of force control have since been proposed, one good example would the Series Elastic Actuator (SEA) which was proposed by the MIT legged locomotion group [19-23]. This thesis, however, builds on the work done on the Series Damper Actuator (SDA). A literature review in chapter 2 would provide more background knowledge and information about force control and force control actuators.

1.2 Motivation

Amongst the various force control actuator systems, a system similar to the SEA was proposed; the Series Damper Actuator. It was demonstrated to have high force fidelity, low output impedance, large force range, and high impact tolerability [24, 25]. In implementing the system, a Magneto-Rheological (MR) fluid damper was used to fulfil the design criteria of using a damper with variable damping coefficient. However, the extra dynamics of the MR fluid damper increased the order of the SDA, thus limiting the bandwidth of the system [25, 26].

Whilst improvement to the initial bandwidth was made through the implementation of a more advanced controller to compensate for the extra dynamics of the MR fluid damper [25], an alternative solution is to use a hydraulic damper with ideal viscous damping properties.

In addition to possessing ideal viscous damping properties, it should also possess the following properties in order to match the original design goals of the SDA.

- The damper should be a continuous rotary (unlimited range of rotation) damper for implementation in a revolute joint.

- Possess a variable damping coefficient (as with the MR fluid damper).
- The damping coefficient should range from very small (near zero) to very large, so that the final actuator system would be capable of high force output.

While there are several types of commercial dampers available, the desired properties for the damper to be used are rather specific, making most of the commercial dampers unsuitable for use in the SDA. As such, there is much value in looking into the mechanical design for such a damper.

1.3 Thesis Contribution

In this thesis, we present 2 design concepts of continuous rotary dampers that may allow for a better implementation of the SDA. In addition to possessing the advantages of a variable damping coefficient, it would also possess close to ideal viscous damping properties.

This thesis would also present experimental data obtained by running test on 2 prototypes fabricated based on these design concepts. An analysis was made to see if the prototypes managed to fulfil the desired properties mentioned in the motivation.

1.4 Thesis Outline

Chapter 1 gives a brief introduction to the motivation of the thesis and highlights the main contributions.

Chapter 2 provides more background about force control actuation, as well as the various forms of force control actuation. It focuses on the SDA system, as well as some background into dampers.

Chapter 3 describes the damper designs conceived. The concept and inspiration behind the design is explained, as well as some design considerations that were made.

Chapter 4 presents experimental data obtain from test conducted on the damper prototypes. An analysis was made to determine the damping properties of the prototypes, as well as assess if the designs are successful in achieving the desired damping properties.

Chapter 5 concludes with a summary, as well as possible work future research that could be conducted.

Chapter 2 - Background and Related Work

2.1 Force Control and its Applications

Force control is necessary for controlled interaction between a robot and an external unknown environment [27-29]. With that consideration, several force control strategies have been developed.

Stiffness control: This is a control strategy in which the robot emulates a spring through a stiffness in the workspace [30]. The input to the system is a desired position; joint torque is calculated from the position error and the force measured at the end-effector.

Damping control: Similar to stiffness control, except that the robot now emulates a damper; this is an integrating controller where the force feedback is used to modify velocity [27]. It is commonly used to damp out disturbances and improve system stability [31, 32].

Impedance control: This control strategy generalizes the ideas of stiffness and damping control [33, 34]. For impedance control, the endpoint emulates an elastic-damping system. The desired position and velocity is modified using position, velocity and force feedback, and in turns modifies the mechanical impedance of the robot. Impedance control, however, does not track a force trajectory, although some modification to the controller can make it possible [35].

Admittance control: This control strategy is based on the concept of using a position control robot as a the baseline system and modifying the admittance of the system to

track a force trajectory [36]. It is a form of explicit force control in that the input and output is force. It is mainly for force tracking in contrast to impedance control.

Hybrid position/force control: This control strategy combines conventional position and force control by defining the workspace as two separate orthogonal workspaces for displacement and force [37]. A proposed variant on this system is the hybrid impedance control which is more flexible in that the impedance can be selected [38].

Explicit Force Control: In this control strategy the measured force is used directly for feedback to form the force control vector [39]. The force control law is normally chosen as one of the subsets of PID [40]. Admittance control, which is also position based, is a form of explicit force control. Explicit force control can also be completely based on force feedback alone.

Implicit Force Control: This control strategy completely excludes force feedback, using only position feedback to achieve a force output [27, 32]. The joint servo positions are predefined for a desired force and feedback gain is determined such that the robot can obtain a particular stiffness.

2.2 Force Control Implementations

Force control can be applied to many situations; however, the system has to be tailored for the intended task. Many criteria for force control have been proposed [18, 41-43], of which a summary has been made below:

Sufficient bandwidth: To compensate for disturbances, it has to fall within the controllable bandwidth of the system. As such, the controller bandwidth has to be sufficiently large enough to cover a large enough range of disturbances.

Low output impedance: Output impedance is the impedance as experienced from the output, and comprises the robot inertia, damping and stiffness of the robot. In robots with high output impedance, even a small disturbance would result in a large force exerted on the environment. Therefore, low output impedance is necessary to compensate for high frequency disturbances.

High force/torque density: The system should be able to produce sufficient force/torque to support its own mass in addition to exerting sufficient force/torque on the environment. Ideally, an actuator of low mass would be capable of producing high force, i.e. high force/torque density.

The following section provides a brief summary of some implementations of force control. While all have achieved force control successfully, each has some drawbacks in relation to the criteria mentioned above.

2.2.1 Conventional Method

The conventional and most popular way to implement force control is use a strain gauge to obtain the force signal [44-47]. The sensor is usually located at the end-effector of the robot where the interaction force is to be controlled. Using the feedback from this sensor, a closed-loop controller would be built to control the actuators of the system to generate the desired force at the end-effector.

However, force sensors are known to have low signal-to-noise ratio, which results in a poor control performance of such a system. The noise can be reduced through the use of a low pass signal filter, although doing also compromises system performance as the filter distorts the original signal; this is particularly true when the signal band is close to

that of the noise. Traditional position and velocity control robots are also designed to be as stiff as possible, making them unsuitable for use in situations where compliance is needed.

Another problem faced by robotic force control is dynamic non-colocation [8, 48, 49]. The problem arises when the sensor and actuator are physically located at different locations along a flexible structure, resulting in unstable modes in the closed-loop system.

2.2.2 Direct drive Actuator

The direct drive actuator is an ideal force source that generates force proportional to the input current to the actuator. It overcomes the non-colocation problem by rigidly connecting the sensor directly to the actuator [50, 51]. The actuator does not employ a gear transmission and as such, the link inertia is kept low. However, in order to generate high torque at low speeds, the armature core of such an actuator has to be made much larger with more windings, increasing the size and weight of such actuators. As such, the impedance of the robot is increased.

2.2.3 Series Elastic Actuator (SEA)

The concept of compliant robot force controlled actuation eventually appeared in the form of the SEA [19, 21]. In the SEA, the output is connected to the motor via an elastic element. At high frequency, this limits the actuator impedance to the stiffness of the elastic element. Also, the output force can be controlled via controlling how much the elastic element is compressed or stretched, turning the force control into a position control problem.

The introduction of the elastic element also has some disadvantages. Whilst the elastic element increases the compliance of the system, it also decreases the bandwidth of the system. Also, the stiffness selected for the elastic component is usually based on a trade-off between the force bandwidth, force range and impact tolerance.

2.2.4 Variable Stiffness Actuator

The stiffness of traditional SEA is fixed, which limits its performance. A high stiffness would allow for higher force range, but lower impact tolerance; the converse is true for a low stiffness value. The VSA is the result of research to overcome this issue by allowing for a variable and controllable stiffness factor [52-54].

2.2.5 Micro-macro Motor Actuator

The parallel micro-macro concept was introduced to overcome force control limitations of actuators [42, 55, 56]. Zinn proposed the Distributed Macro-Mini (DM^2) actuator [42, 56], which combined the SEA with the micro-macro actuator to solve the low bandwidth problem of the SEA.

The macro actuator is a SEA with low output impedance but a low controllable bandwidth. The mini actuator is a small, single stage gear transmission actuator, which is used to compensate for the phase of the macro actuator. While this system results in a relatively low output impedance and high bandwidth, it is only effective when the mini-actuator is not saturated. If the mini actuator is saturated, the bandwidth of the system would become close to that of the SEA macro actuator.

2.3 Series damper actuator (SDA)

The SDA was proposed by Chew [24] as an alternative solution to the SEA in achieving force control actuation. The SDA system consists of a motor, gear transmission and a damping component connected in series in that order. Contrary to the SEA system, which controls the force output via the compression of the spring, the SDA controls the force output by varying the relative velocity in the damper. The controlled force output can therefore be determined from the following damping force equation:

$$F_D = bv \tag{2.1}$$

where F_D is the damping force, b is the damping coefficient, and v is the input velocity to the damper.

By using a damping element, the SDA is first order system, as a later section will show. The SDA also has an advantage in that the damping coefficient of the damping element can be easily made variable through the design of the damper. For example, the current implementation of the SDA is based on using a MR fluid damper, which allows for variable damping. This allows for higher force fidelity at both high and low force ranges; at high and low force ranges, the damping coefficient can be increased and decreased respectively. The dissipative nature of the damping element also allows for good impact absorption.

The following five sections present the analysis made by Zhou [25] of the SDA, as well as the MR fluid damper so as to provide a better understanding of the SDA.

2.3.1 SDA Model

This subsection presents a model for the SDA [25]. Figure 2.1 and Figure 2.2 are the SDA model and frequency block diagrams.

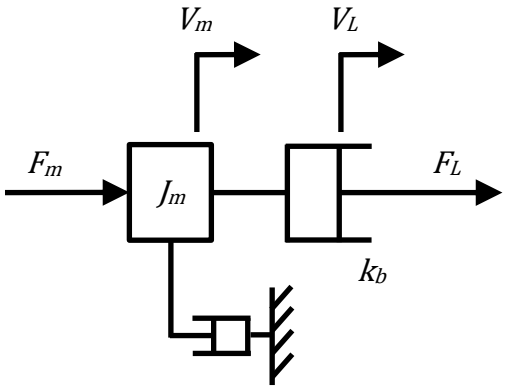

Figure 2.1: The SDA model

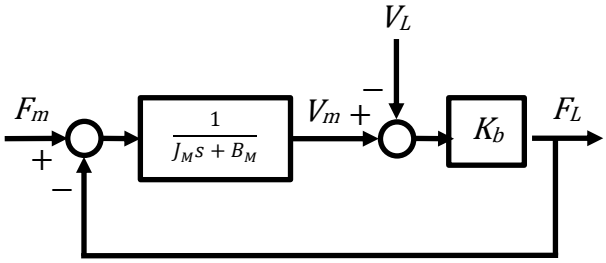

Figure 2.2: Block diagram of SDA plant

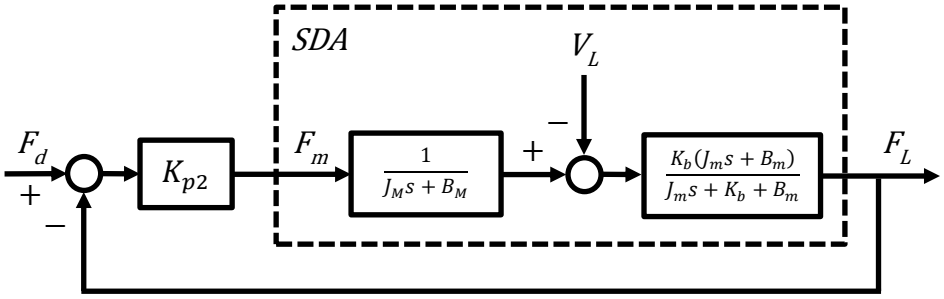

Figure 2.3: Block diagram of SDA control system with a unit feedback and a proportional controller

Based on the model, the dynamic equations of the SDA plant are as follows:

$$F_L = K_b(V_m - V_L) \tag{2.2}$$

$$F_m - F_L = J_m \dot{V}_m + B_m V_m \tag{2.3}$$

where F_L is the output force of the actuator; K_b is the damping coefficient; V_m is the motor rotor velocity; V_L is load capacity; F_m is the magnetic force applied on the motor; J_m is the motor inertia; B_m is the motor damping constant.

Combining equations 2.2 and 2.3 and taking the Laplace Transform, the plant transfer function can be found to be as follows

$$F_L(s) = \frac{K_b}{J_M s + B_m + K_b} F_m(s) - \frac{K_b(J_m s + B_m)}{J_m s + B_m + k_b} V_L(s) \quad \text{2.4}$$

Here, Zhou assumes that the control law is of the proportional type [25], which would yield the closed loop system block diagram as shown in Figure 2.3. As such, the following equation can be obtained.

$$F_L(s) = \left\{ \frac{K_{p2}}{J_m s + B_m} [F_d(s) - F_L(s)] - V_L(s) \right\} \frac{K_b(J_m s + B_m)}{J_m s + B_m + k_b} \quad \text{2.5}$$

where K_{p2} is the proportional gain.

From equation 2.5, the closed-loop transfer function of the SDA can be found to be

$$F_L(s) = \frac{K_{p2} K_b F_d(s) - K_b(J_m s + B_m) V_L(s)}{J_m s + B_m + K_b(K_{p2} + 1)} \quad \text{2.6}$$

2.3.2 System Bandwidth

Assuming the actuator output end is fixed, the load velocity V_L in equation 2.6 would be zero. The closed loop transfer function [25] would hence be expressed as

$$G_{cl} = \frac{F_L(s)}{F_d(s)} = \frac{K_{p2}K_b}{J_m s + B_m + K_b(K_{p2}+1)} \quad 2.7$$

Assuming that the motor rotor damping is small and therefore can be neglected, the above equation can be further simplified to the following:

$$G_{cl} = \frac{K_{p2}K_b}{J_m s + K_b(K_{p2}+1)} \quad 2.8$$

By manipulating the above equation, the following form can be obtained:

$$G_{cl} = \frac{K_2 \omega_{n2}}{s + \omega_{n2}} \quad 2.9$$

where the controlled natural frequency is

$$\omega_{n2} = \frac{K_b(K_{p2}+1)}{J_M} \quad 2.10$$

and

$$K_2 = \frac{K_{p2}}{K_{p2}+1} \quad 2.11$$

From equation 2.9, it can be seen that the SDA is a first order system. If the proportional controller gain K_{p2} is sufficiently large (i.e. $K_{p2} >> 1$), K_2 would approach unit and the SDA system closed loop bandwidth would be ω_{n2}. Therefore, from equation 2.10, it can

be seen that the bandwidth of the system can be increased by increasing the damping constant (K_b) and the proportional controller gain (K_{p2}).

2.3.3 Output Impedance

When the input force $F_d(s)$ is zero, the SDA transfer function (equation 2.6) can be written as:

$$Z(s) = -\frac{F_L(s)}{V_L(s)} = \frac{K_b(J_m s + B_m)}{J_m s + B_m + K_b(K_{p2} + 1)} \quad 2.12$$

Equation 2.12 is the expression for the output impedance of the system. Assuming $B_m << K_b(K_{p2}+1)$, equation 2.12 can be rewritten as:

$$Z(s) = K_b \frac{s}{s + \omega_{n2}} \quad 2.13$$

From equation 2.13, it can be shown that the output impedance at low frequency is ideally zero and increases with increasing frequency. At high frequency, it would approach the damping constant K_b. The output impedance can be effectively decreased by decreasing the damping coefficient.

2.3.4 System efficiency

The efficiency of a system is defined as the ratio of the system output power to input power. If the subsystems are connected in series, then the system efficiency can be found by taking the product of the efficiencies of the individual subsystems. In this case, the efficiency of the SDA can be found by taking the product of the motor efficiency (η_m) and the efficiency of the damping component (η_d).

Looking at the damping component, neglecting inertia, the constitutive equations of the damper (assumed to be viscous in nature) are given below:

$$F = K_b(V_m - V_L) = K_b \Delta V \quad (2.14)$$

$$F = F_L \quad (2.15)$$

where F is the output force of the damper and ΔV is the difference between V_m and V_L.

The power dissipated in the damper is therefore

$$\Delta P = F \Delta V = \frac{F_L^2}{K_b} \quad (2.16)$$

It can be seen from equation 2.16 that if there should there be an upper boundary of power dissipation defined, then the damping constant would also be bounded. Thus, for some defined maximum output force F_{max} and some defined maximum power dissipation ΔP_{max}, the minimum value for the damping coefficient can be found to be

$$K_b \geq \frac{F_{max}^2}{\Delta P_{max}} \quad (2.17)$$

The efficiency of the damper is

$$\eta_d = \frac{P_L}{P_m} = \frac{F V_L}{F V_m} = \frac{V_L}{V_m} \quad (2.18)$$

where P_L is the output power of the damper and P_m is the output power of the motor.

Combining equations 2.14 and 2.18 gives

$$\eta_d = \frac{P_L}{P_m} = \frac{V_L}{V_L + \Delta V} = \frac{K_b V_L}{F_L + K_b V_L} \quad 2.19$$

So, the overall efficiency of the SDA is the product of the motor efficiency (η_m) and the efficiency of the damping component (η_d), i.e.

$$\eta = \eta_m \eta_d = \eta_m \left(\frac{K_b V_L}{F_L + K_b V_L} \right) \quad 2.20$$

According to equation 2.20, for high output force and velocity, the SDA would perform more efficiently. Conversely, the system efficiency is low with low output force and velocity. In addition to output force and velocity, the damping coefficient also has effect on the efficiency of the system; the higher the K_b value, the more efficient the system is. As K_b approaches infinity, the efficiency of the damper approaches. This is understandable as the damper would simply be behaving as a rigid link.

2.3.5 Impact Tolerance

For impact tolerance, the interaction energy that is transferred from the environment to the actuator is considered. Assuming that there is a sudden load motion V_L on the output of the actuator, the impact power due to the load force and load velocity at the system output is:

$$P_L = F_L V_L \quad 2.21$$

Combining equations 2.21 and 2.12 and neglecting the minus sign in the latter, the expression for the controlled impact power P_L is

$$P_L(s) = \frac{V_L^2(K_b J_m s + B_m)}{J_m s + K_b(K_{p2}+1)B_M} = V_L^2 K_b \frac{s+\sigma\omega_{n2}}{s+\omega_{n2}} \quad 2.22$$

where

$$\sigma = \frac{B_m}{K_b(K_{p2}+1)} \quad 2.23$$

Equation 2.22 is just the power generated at the damper output by the impact velocity V_L. The power transmitted to the motor, P_{cp} is

$$P_{cp} = P_L(s) - \Delta P(s) \quad 2.24$$

Substituting equations 2.16 and 2.22, equation 2.24 can be rewritten as

$$P_{cp} = V_L^2 K_b \left[\frac{s+\sigma\omega_{n2}}{s+\omega_{n2}} - \left(\frac{s+\sigma\omega_{n2}}{s+\omega_{n2}}\right)^2\right] = V_L^2 K_b \left[\frac{(s+\sigma\omega_{n2})(1-\sigma)\omega_{n2}}{(s+\omega_{n2})^2}\right] \quad 2.25$$

Define

$$G_{cp}(s) = \frac{(s+\sigma\omega_{n2})(1-\sigma)\omega_{n2}}{(s+\omega_{n2})^2} \quad 2.26$$

Neglecting σ and normalising equation 2.26 with ω_{n2} gives

$$G_{cp}(S) = \frac{S}{(S+1)^2} \quad 2.27$$

Therefore,

$$P_{cp}(s) = V_L^2 K_b G_{cp}(S) \quad 2.28$$

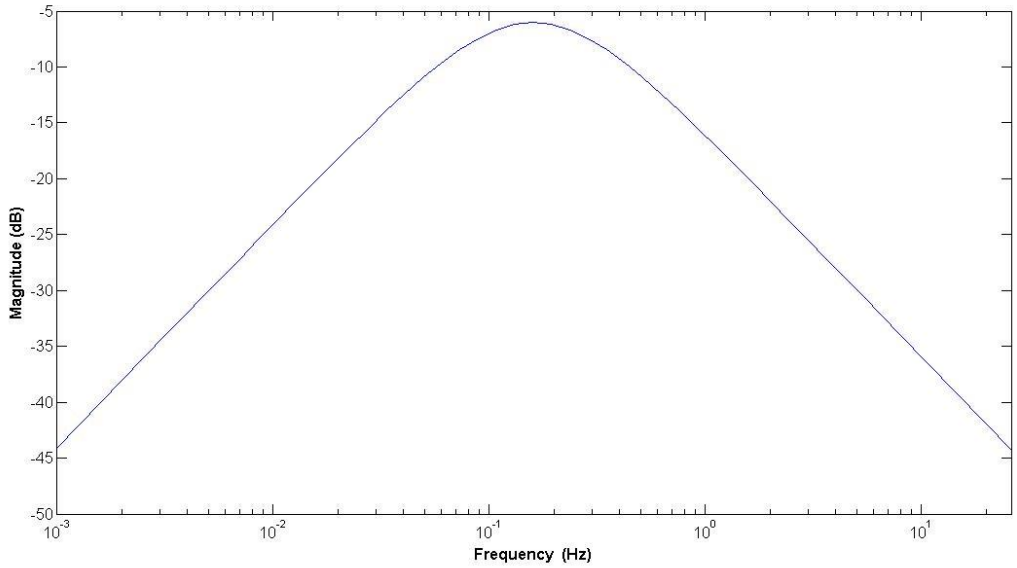

Figure 2.4: Frequency Response of $G_{cp}(S)$

Figure 2.4 shows the frequency response of $G_{cp}(S)$; it can be seen that at high and low frequency, the power transferred to the motor is very small. This means that the damper absorbs all the impact. At the controlled natural frequency, P_{cp} is at its maximum. Equation 2.28 also indicated that P_{cp} is proportional to K_d for a constant value for the controlled natural frequency. Thus, decreasing K_d effectively decreases the amount of impact energy being transmitted to the motor.

2.4 Summary

This chapter has provided an overview of the various methods of force control, as well as several forms of their implementation. While all are successful at achieving force control, each form of implementation has their advantages and disadvantages.

Much attention was spent on the SDA as it is the focus of this research. An analysis of the SDA system was provided to illustrate the properties of the SDA; by controlling the damping coefficient of the damping component of the SDA, the controllable bandwidth,

output impedance, system efficiency and impact tolerance can be controlled. A high damping coefficient would allow for a wider controllable bandwidth and better system efficiency, at the cost of higher output impedance and lower impact tolerance. Conversely, decreasing the damping coefficient would result in a lower output impedance and better impact tolerance, but result in a smaller controllable bandwidth and less efficient system.

While there seems to be a trade-off between controllable bandwidth, output impedance, impact tolerance and system efficiency for a particular value of the damping coefficient, by using a damping component with a variable damping coefficient, the SDA would be a versatile force control actuator and applicable at both low and high force applications.

Chapter 3 - Damper Design

Chew and Zhou [24] proposed and implemented the SDA using an MR fluid damper. It succeeded in showing that the SDA system could achieve very good output force fidelity. By using an MR fluid damper, the damping coefficient of the system could be adjusted, demonstrating the versatility of the SDA system. However, it was noted that there were some short-comings in using the MR Fluid damper.

In order to design a viscous damper with linear damping properties, it would be necessary to take a look at damping as a whole, as well as commercial viscous dampers that are already available.

3.1 Damping

Damping is the phenomenon by which mechanical energy is dissipated in dynamic systems, usually by conversion into internal thermal energy [57]. Several types of damping are inherent in all mechanical systems; should these forms of internal damping be insufficient for the proper functioning of the system, then external dampers can be added to the system.

There are three primary mechanisms of damping in mechanical systems:

Internal damping: The damping effect originates from energy dissipation associated with microstructure defects such as grain boundaries and impurities in the material, thermo-elastic effects due to temperature gradients, eddy-current effects in ferromagnetic materials, and dislocation motion in metals.

Structural damping: This is the result of mechanical energy dissipation caused by friction between components at common points of contact joints or support in a mechanical structure.

Fluid damping: This form of damping occurs when a mechanical component moves through a fluid medium. The local displacement of fluid due to the fluid-structure interaction results in a drag force on the moving structure. This resistance is the cause of mechanical energy dissipation in fluid damping.

In order to improve the damping properties of a mechanical structure, external dampers may be added. Often, dampers are used to damp out vibrations in buildings and machines. One example of their use is integration into building structures to dissipate energy that would otherwise damage the building. This is useful in earthquake regions, or in very tall buildings to damp out oscillations caused by strong winds. Other common uses of dampers are on doors and as vehicular shock absorbers.

There are two general types of dampers: passive dampers and active dampers. Passive dampers are devices that dissipate energy through some kind of motion, without the need of some external source of power or actuation. Active dampers have actuators that need external sources of energy, and operate primarily by actively controlling the motion of the system that needs damping.

As the described before, the damper in the SDA should be passive and fluid damping in nature, thus only such dampers would be considered in the design process. The following section takes a look at commercially available viscous dampers as a source of inspiration for the design process.

3.2 Typical Commercial Dampers

Viscous dampers are commonplace in many mechanical structures; most commonly, they are seen in vehicles as shock absorbers or in machinery such as washing machines. They are found in two forms; linear acting pistons and rotary forms.

3.2.1 Linear acting pistons

Figure 3.1: Examples of linear acting piston dampers

Linear acting piston dampers are the most common type of dampers, and are very simple in construction and working principle. As their name implies, they operate only along one axis. They are usually used together with springs in car shock absorbers, and come in a variety of sizes.

Linear acting piston dampers operated on the principle of moving a piston through a fluid medium, as shown in Figure 3.2. Orifices are machined into the piston or piston chamber wall. As the piston is forced into the piston chamber, the damper fluid is pressurized and forced to flow through the

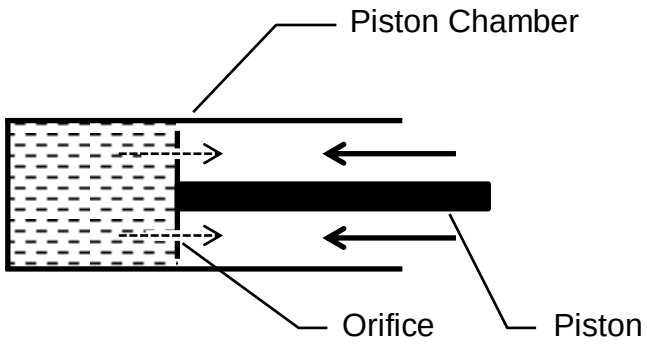

Figure 3.2: Linear acting piston damper sectional view

orifice. The pressure of the damper fluid is dependent on the cross-sectional area of the orifice, and it is this pressure that provides a force output on the piston shaft.

3.2.2 Rotary dampers

Figure 3.3: Examples of rotary dampers

Converse to piston dampers, rotary dampers operate by rotation about a single axis. While they are also used in vehicles, they are more commonly used with hinges to prevent doors or lids from swing too fast. There are two types of rotary dampers: continuous and non-continuous.

Non-continuous rotary dampers (NCRD) are similar to piston dampers; the damping effect is generated by moving a vane through a fluid medium. The extent of the damping effect is controlled by varying the orifice size through which the fluid flows. However, due to the damper design, the damper cannot rotate past 360º; most such dampers are able to rotate about 120º.

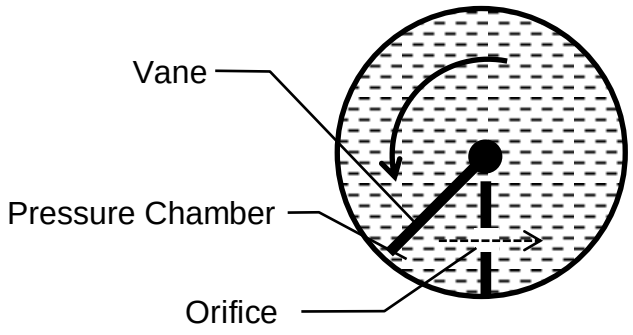

Figure 3.4: Non-continuous rotary damper sectional view

Continuous rotary dampers (CRD) are dampers that are able to rotate freely past 360º. However, commercially available CRDs are different from their non-continuous counterparts in that they operate on the principle of viscous shear. The CRD usually consists of a highly viscous fluid medium sandwiched between the rotor and the stator plates. As the rotor rotates, the fluid experiences a shear, which then results in the dissipation of energy from the system. The shear in the fluid is proportional to the viscosity of the fluid medium, as well as inversely proportional to the distance between the two plates. By controlling the distance separating the two plates or the viscosity of the fluid medium, the damping coefficient can be controlled.

3.2.3 MR fluid damper

The MR fluid damper is an example of a CRD. While most commercial CRDs control their damping coefficient by controlling the distance separating the rotor and stator plates, the MR fluid damper controls the damping coefficient by varying the viscosity of the MR fluid medium. This is done via varying the strength of a magnetic field passing through the MR fluid; the viscosity increases with magnetic field strength.

This makes the MR fluid damper suitable for use in the SDA for two reasons; first, being continuous, it is able to produce force output for an indefinite amount of time. Piston dampers and NCRDs have limited range of motion; once the vane or piston reaches the end of the compression chamber, no more damping can be achieved. Second, the MR fluid damper can change its damping coefficient via the damper is still in operation.

However, the MR fluid damper has some drawbacks. Zhou, in his initial implementation of the MR fluid damper actuator, first neglected the dynamics of the MR fluid damper

[25]. He noticed that due to the dynamics of the MR fluid damper, the order of the final system had increased. This resulted in phase delay of the system output and therefore, a lower system bandwidth. He later used an improved model of the MR damper, and with a more delicate controller, managed to improve the bandwidth of the system.

3.3 Design Goals

In order to improve on the SDA system, it is proposed that the MR fluid damper be replaced by a viscous damper with linear damping properties. However, it can be seen that commercial dampers are unsuitable for the task. Dampers which operate on the hydraulic effect are not continuous; as such, they would not be able to produce continuous force/torque if implemented in the SDA. CRDs available are based on fluid shear rather than hydraulic effect. With the exception of the MF fluid damper, the damping coefficient of such dampers cannot be varied while the damper is in operation.

As such, a new damper should be designed to fit the SDA. This damper should possess the following properties:

- The damper should be a viscous damper with linear damping properties. This would make for easier implementation.
- The damper should be a CRD. The resulting SDA implementation would be able to have continuous force output.
- The damper must have a variable damping coefficient, and the damping coefficient should be variable over a very large range. This would allow for a versatile actuator capable of operating at high and low force output.

The following section presents two concepts on which designs were based. The first concept is based on the conventional non-continuous damper, with modifications made to make the damper continuous. The second concept is a novel design based on the concept of displacement pumps.

3.4 Continuous Rotary Vane Damper (CRVD)

In 2005, some work was done to design a rotary damper with a variable damping coefficient [1]. The basic premise was to consider the conventional non-continuous rotary damper and make modifications to the design so as to make it continuous.

3.4.1 Non-continuous Rotary Damper (NCRD): Revisited

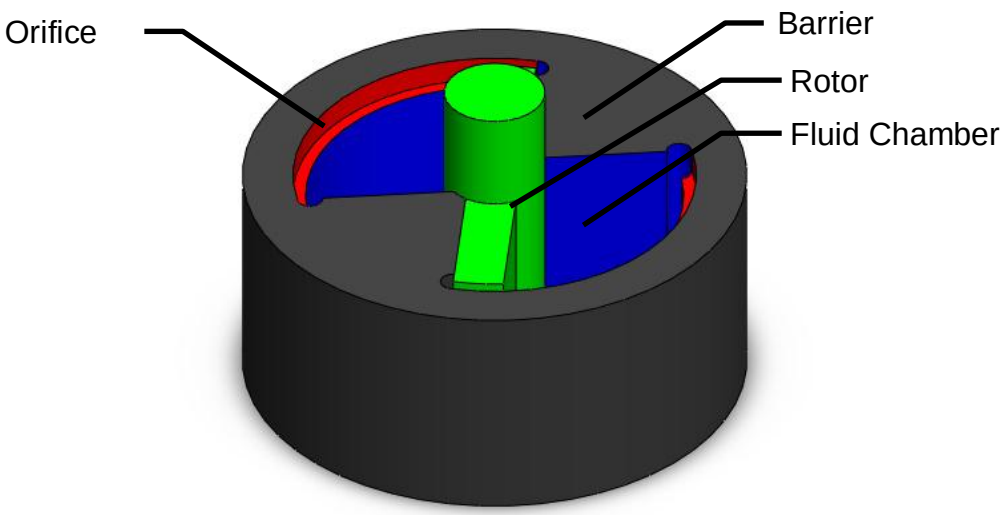

Figure 3.5: 3D drawing of a NCRD

Figure 3.5 is a 3D drawing of a typical NCRD. The green component is rotor, which comprises two vanes affixed to the input shaft. The blue regions are the fluid chambers separated by fluid barriers, and the red region is the orifice.

Figure 3.6 illustrates the flow of the damping fluid as the vane moves in the damper. As the rotor shaft is turned counter-clockwise, the fluid in the fluid chamber is pressurized. Due to this pressure, the fluid flows through the orifice section. By varying the cross-sectional area of the red section, the pressure generated in the fluid chamber can be controlled, hence controlling the damping coefficient.

There are several benefits of designing the damper this way. First, the vane is moving through a mostly stationary fluid medium; the fluid would not gain momentum. Secondly, the damper would be easy to manufacture and assemble.

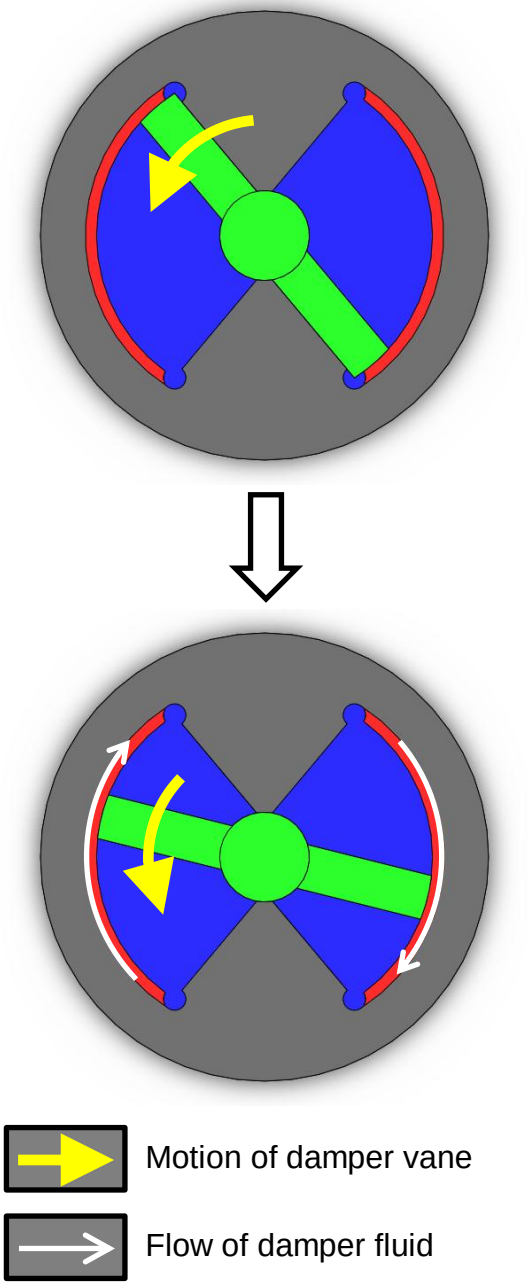

Figure 3.6: Flow of damper fluid during damper operation

However, these design considerations make the NCRD unsuitable for use in the SDA system. In order to pressurize the fluid, the damper has been designed to have two separate chambers separated by fixed walls, hence restricting the range of rotation. Furthermore, as the orifice is formed by cutting a

groove into the wall of the fluid chamber, it is difficult to implement an orifice with a variable cross-sectional area.

3.4.2 The CRVD Design

To make the NCRD into a CRD whilst retaining its viscous damping properties, some modifications to the NCRD were proposed by Chang in 2005 [1]. Firstly, the orifice was redesigned to be in the wall separating the fluid chambers. This way, the orifice could be made adjustable by controlling the cross-sectional area of the orifice. Secondly, the rotor had to be designed such that the vanes could retract and extent to avoid the chamber wall during operation. As such, the new damper design would be referred to as the continuous rotary vane damper (CRVD) in order to differentiate itself from the conventional NCRD and CRD.

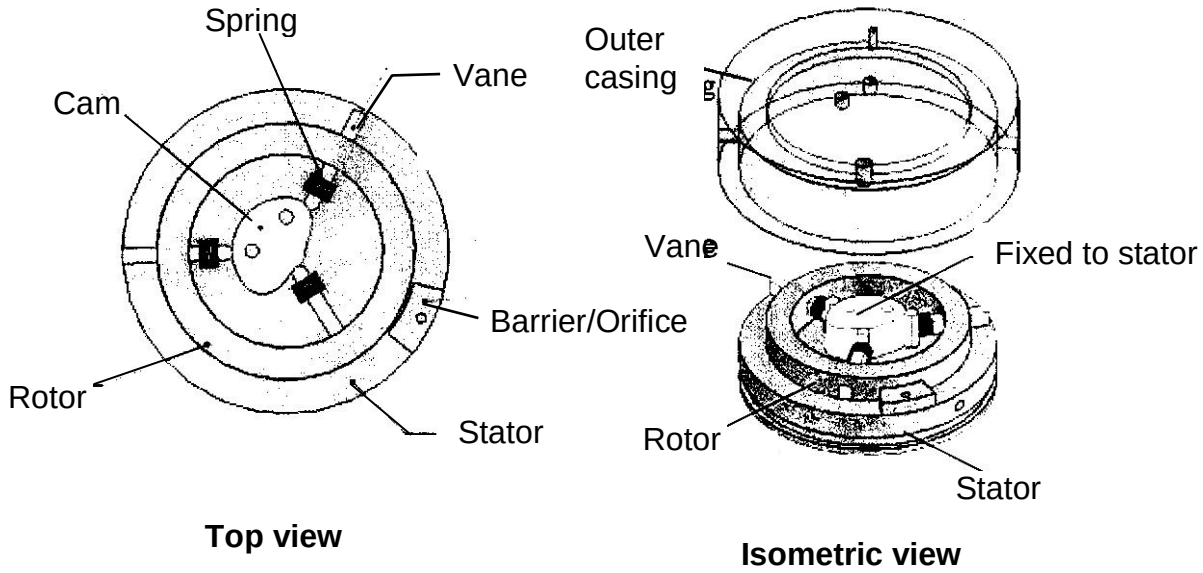

Figure 3.7: Drawing of rotary damper with variable damping effect designed by Chang [1]

Figure 3.7 is the drawing of the damper designed by Chang. As can be seen from the drawing, he intended to control the movement of the vanes through the use of a cam, which is a sound plan considering that the damper will be executing rotational motion.

Chang made the following design decisions:

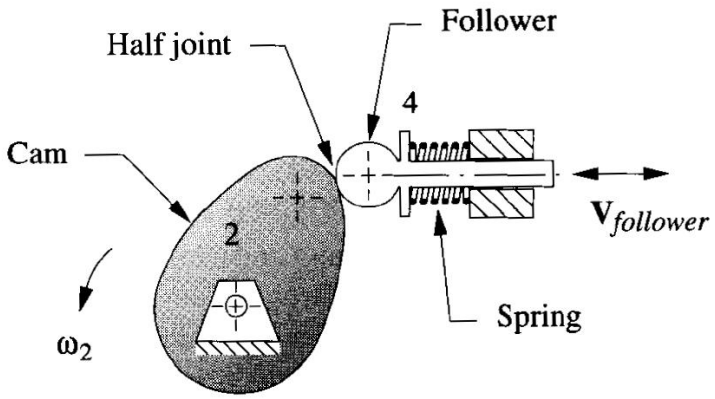

Figure 3.8: Diagram of a force-close cam system [58].

Implementation using a force-closed cam: In a force-closed cam system (as shown in Figure 3.8), the cam is responsible for only motion in one direction; the force for the return direction is contributed by some other component, such as a spring. Chang opts for this cam system for several reasons. First, the cost of manufacturing a force-closed cam system is lower. Secondly, force-closed cam systems are generally smoother in motion as the cam follower is in constant contact with the cam. However, as it has a spring system, the system may undergo resonance at high speeds. As the SDA implementation is ideally run under low speed conditions, this drawback is not an issue.

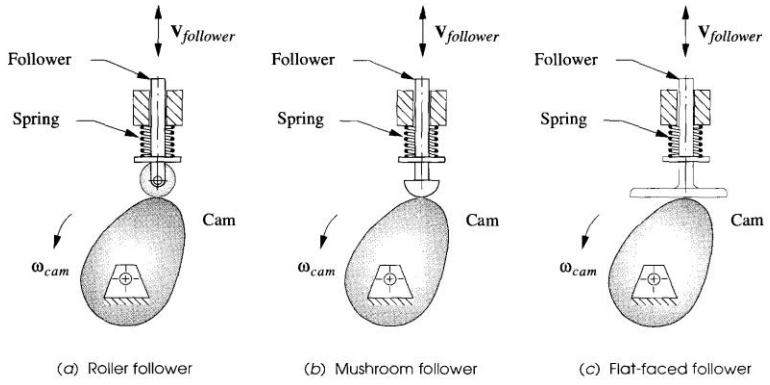

Figure 3.9: Types of cam followers [58].

Implementation using a mushroom follower: Chang selected the mushroom cam follower as it can accept a negative curvature on the cam, allowing for a simpler consideration for the cam profile. While a roller follower would have been better as it would have resulted in less friction against the cam, it is possible that he did not consider it for cost, sizing and simplicity sake.

O-ring sealing: As the damper operates using a fluid medium, it is necessary to seal the fluid in the device in order for the system to operate properly. To do so, Chang used two O-rings; one O-ring was situated between the rotor and stator, and the other was situated between the stator and outer casing.

3.4.3 Problems faced by the CRVD design

In his implementation of the CRVD design, Chang faced two main problems. Firstly, the damper experienced high friction due to the O-ring sealing. Secondly, the damper prototype jammed frequently during initial inspection, even with no hydraulic fluid present in the damper. By inspecting his design closely, several reasons for these can be offered.

Sealing: In his design, Chang used O-rings in all his sealing. However, O-rings are static seals; they are meant to be placed in locations where there is no excessive movement of the sealing counterfaces [59]. As a result, there is a high amount of friction in the rotor/stator interface. It would also be highly likely that the O-ring seal would sustain damage over time, reducing the effectiveness of the seal. He should have in fact used a rotary seal. Furthermore, the seal was at a location of large circumference. This increases the contact area between the interfering surfaces, which also increases the friction.

Cam pressure head: The cam pressure head is defined as the angle between the direction of motion of the follower and the direction of the axis of transmission (refer to Figure 3.10). In general, it is desirable to keep the pressure angle between zero to 30^0 for translating followers; beyond that, the sliding friction would increase to levels that would jam the follower [58]. Chang had considered this in his design; his pressure angle is about 28^0 [1]. However, while it may be within the guidelines, it is considerably close to the upper limit.

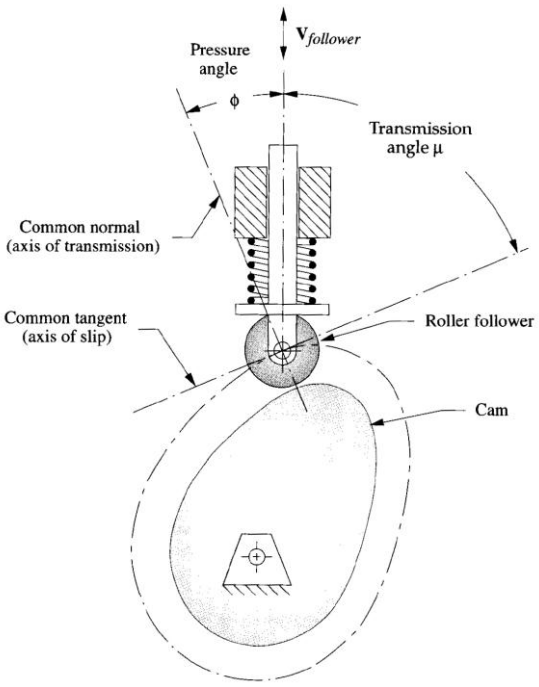

Figure 3.10: Various angles in the cam system [58]

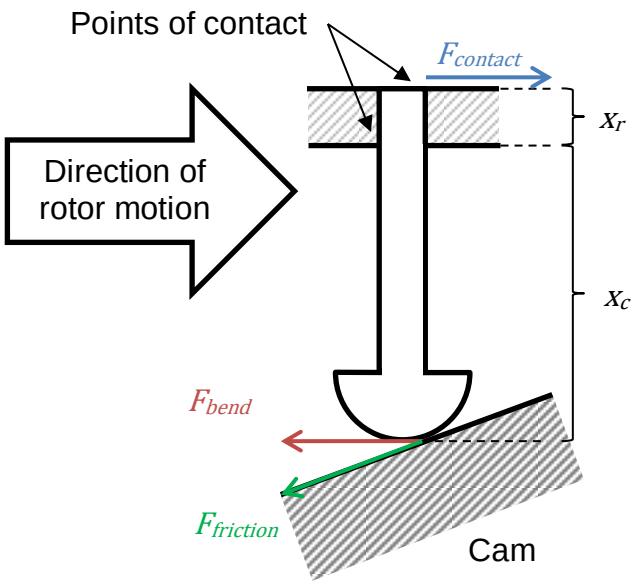

Figure 3.11: Figure of contact forces between rotor, cam and cam follower

Rotor design and dimensions: The rotor in the 2005 CRVD was designed as a hollow cylinder in order to accommodate the internal cam. However, this has two problems. First, the rotor shape is irregular and would be rather hard to manufacture. Secondly, as the cam follower is rather long in comparison to the rotor wall thickness, when the cam follower is fully retracted, there are high contact forces between the rotor and cam follower due to long moment arm. An expression for the contact force between the cam follower and cam can be found as follows:

$$F_{contact} = \frac{x_c}{x_r} F_{bend} \qquad 3.1$$

where $F_{contact}$ is the contact force between the cam follower and the rotor; F_{bend} is the bending force on the cam follower (resolved from the frictional force between the cam follower head and cam wall); x_c is the distance between the cam and rotor surfaces; x_r is the rotor wall thickness.

As can be seen from Figure 3.11 and equation 3.1, the larger the ratio between the rotor wall thickness and the cam/rotor surface distance, the larger the contact force will be. High contact force will have two effects. First, the friction between the cam follower and rotor will be high, impeding the movement of the cam follower. Second, the high force may result in the cam follower bending, which will prevent the follower from sliding properly into the rotor. Both effects will result in the rotor becoming unable to turn, and may therefore be a contributing factor to the damper jamming.

Concentricity: One notable observation of the CRVD is that there are no bearings in the design to keep the rotor concentric to the stator. An O-ring was used instead as the interface between the stator and rotor; due to its compliant nature, the stator is likely to have wobbled or tilted within the stator, resulting in both components coming into contact. Furthermore, the CRVD was fabricated using rapid prototyping. While fast and convenient, the surface finishing of the prototype would not have been very good without secondary processes. Contact between the rotor and stator with such rough finishing is likely to have resulted in high friction, which possibly could have cause the damper to jam.

Considering the problems in the CRVD, a revised design was made to overcome the shortcomings faced by the first design.

3.4.4 Modified CRVD (MCRVD) Design

The 2005 CRVD used the NCRD as the base concept and modified the design so that continuous rotary damping could be achieved. To overcome the problems encountered in its design, inspiration was drawn from a similar device: the sliding vane pump.

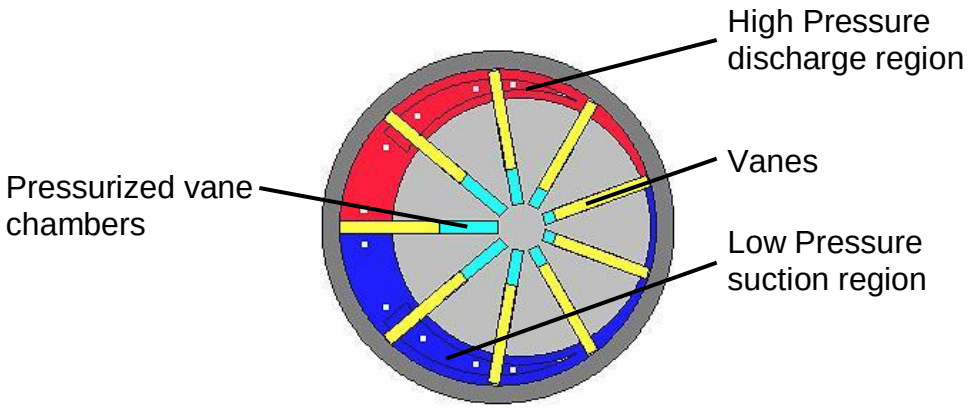

Figure 3.12: Diagram of a vane displacement pump [60]

Figure 3.12 shows a drawing of a vane pump; as the pump rotor rotates clockwise, the pump sucks in fluid at the blue region, and expels fluid at the red, high pressure region. As the rotor rotates, the vanes move radially, as well as slides along the outer housing as it transmit fluid towards the outlet region.

Cam design

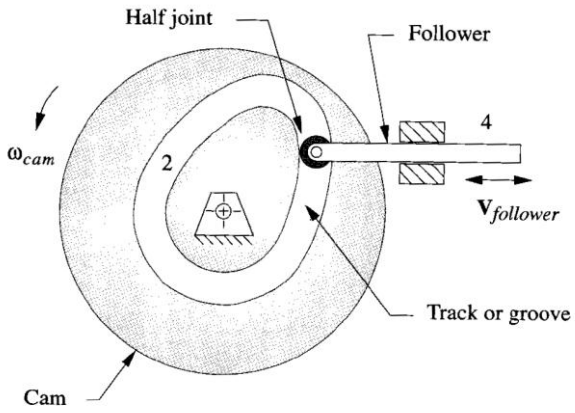

Figure 3.13: Diagram of a form-close cam system [58]

It can be seen that the vane pump operates on a similar principle of what the CRVD hoped to achieve. The vane pump operates using a force-closed cam; the outer casing wall acts as the cam, and pressure diverted from the pump outlet to the vane chambers force the vanes outward. However, this means that the vane pump in this example can only operate in one direction. Springs could be used instead, but doing so may introduce a capacitance component into the system. As such, the MCRVD employs the use of a form-closed cam system instead (Figure 3.13).

The cam follower runs along a groove cut into the cam; the two sides of the groove acts like two cam surfaces. One surface would act to force the vane outward; the opposite surface would act to force the vane inward. One problem associated with the form-close cam system is crossover shock. This occurs when the cam follower switches from one side of the track to the other side of the track, resulting in impact forces [58]. However, as the cam is to operate at low speeds, this crossover force is likely to be low. Furthermore, the crossover force can be reduced by controlling the shape of the cam.

This brings us to the shape of the cam itself. The shape of the groove is important in reducing the pressure angle, as well as ensuring that the vanes clear the orifice during operation. To reduce the pressure angle as much as possible, two considerations were made: first, the cam diameter was to be made as large as possible. Second, the angle over which the rise/drop in profile was to be made as large as possible. All this is to reduce any sharp changes in curvature in the cam profile.

The MCRVD uses a rise-dwell-fall motion program. Rise indicates an increase in the cam profile, fall indicates a decrease in the cam profile, and dwell indicates no change in the cam profile, i.e. no change in output motion for a specified period of input motion.

Figure 3.14 shows the motion program of the cam for the RCRVD. There is a fall from 0^0 to 60^0, rise from 60^0 to 120^0, and dwell for the rest of the cam. The profile of the cam is defined by the following function:

$$L = \begin{cases} \frac{1}{2}(r_o + r_i) + \frac{1}{2}(r_o - r_i)\cos 3\theta & 0° \leq \theta \leq 120° \\ r_o & 120° < \theta < 360° \end{cases} \quad 3.2$$

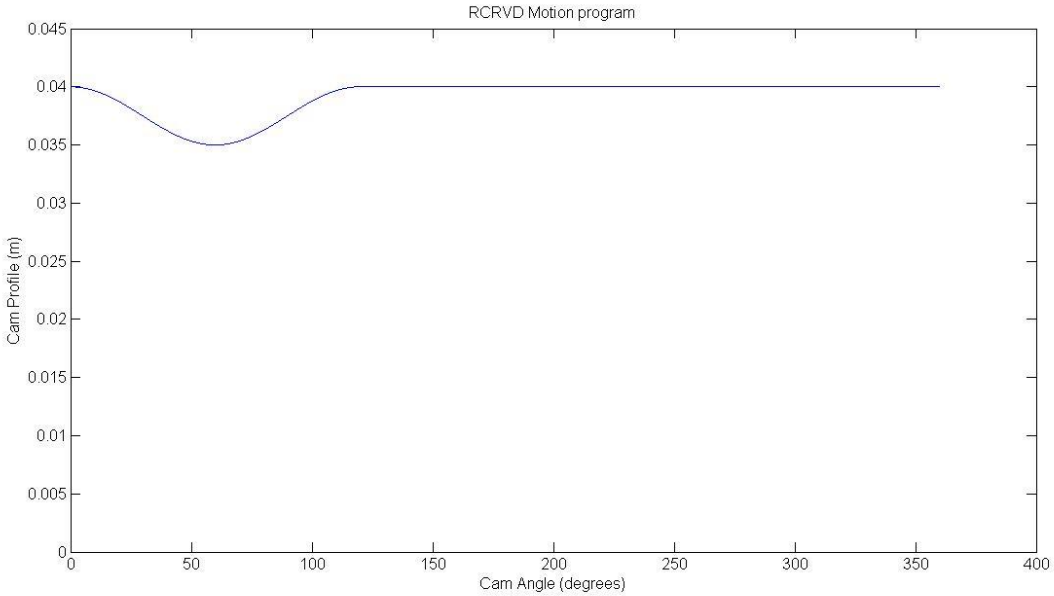

Figure 3.14: RCRVD motion program

By defining r_o as 40mm and r_i as 35mm, the cam profile adopts the shape as shown in Figure 3.15.

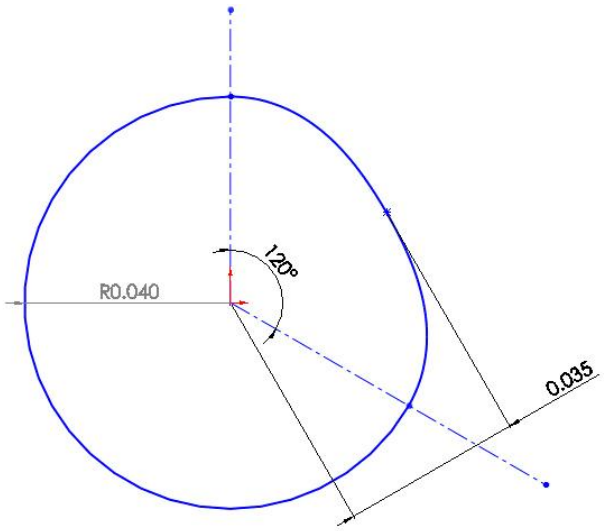

Figure 3.15: Drawing of cam profile for RCRVD

The pressure angle should ideally be as low as possible. From equation 3.2, the expression for the pressure angle ($\theta_{pressure}$) was found to be:

$$\theta_{pressure} = 90° - \cos^{-1}\left(\frac{-3(r_o - r_i)\sin\theta}{\left[\left(r_o^2 + r_i^2\right) + 2\left(r_o^2 - r_i^2\right)(\cos 4\theta + \sin 4\theta + 2(\cos\theta - \sin\theta)\sin 3\theta) + 8\sin^2 3\theta\right]^{\frac{1}{2}}}\right) \quad \textbf{3.3}$$

Figure 3.16 shows the plot of the pressure angle against the cam angle. It can be found that the maximum angle is 9.65º. This is smaller than the pressure angle of the 2005 CRVD.

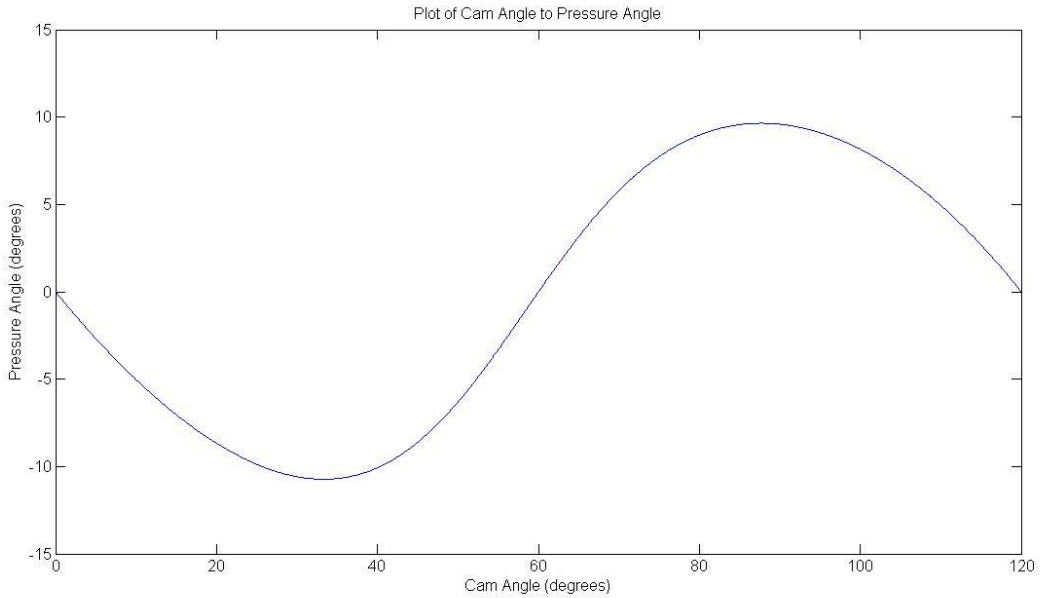

Figure 3.16: Plot of Pressure angle against Cam angle

Sealing design

Apart from the cam design, the seals in the 2005 CRVD were also an issue; an O-ring seal was used as the interacting medium between the rotor and the stator. Not only would this result in high friction, the concentricity of the stator to the rotor would not be maintained.

It is therefore necessary to select the appropriate seals for various surface interfaces in the damper in order to maintain minimal friction in the damper, and still provide adequate sealing to prevent leakage of damping fluid and subsequent loss of fluid pressure. Following is a brief overview of seals and their uses.

Static seals: Static seals include O-ring seals (Figure 3.17), X-section seals, T-section seals, gaskets (Figure 3.18), et cetera to name a few. They are usually used between stationary surfaces, although sometimes O-rings are used in reciprocating applications. They are usually self-energizing[1].

Figure 3.17: O-rings [61]

Figure 3.18: Gasket [61]

Rotary seals: Rotary seals are used to provide sealing between a rotating shaft and its housing. Rotary seals can be self-energizing, fluid energizing[2], or both. A typical example of a rotary seal is the lip-seal.

[1] Self-energizing seals are seals where the material properties provide the energy for the sealing effect. Seals could be made of elastic material like rubber, or have a spring embedded.
[2] Fluid-energizing seals are seals where the pressure from the fluid being sealed provides the energy for the sealing effect. This is mainly accomplished through the design of the seal.

Figure 3.19: Rotary Seals [61]

Reciprocating seals: Reciprocating seals are used to provide sealing between a reciprocating shaft and its housing. These seals are usually made of a combination of elastomer and plastic materials to achieve the necessary energy for sealing.

Figure 3.20: Reciprocating Seals [61]

Based on this knowledge, the sealing for the MCRVD was redesigned to include rotary seals in order to reduce the friction between the rotor and stator, and prevent leakage from this surface interface. An O-ring seal was also used between the stator cover and base to maintain the fluid pressure in the damper.

Other design considerations and fabrication

To the further reduce friction; ball bearings were incorporated into the design to ensure that the rotor is concentric with the stator, and that the rotor will not come into contact with the stator (clearance between the stator and rotor is 0.1mm). The damper was also designed to be modular to make fabrication via conventional means (e.g. CNC machining) possible, as well as make assembly easier. The materials selected for the damper was 6061aluminum for the cam, rotor and stator; and transparent polycarbonate for the lid as that the internal workings can be observed.

Final design for the MCRVD

Figure 3.21 shows a 3D CAD render of the MCRVD, which incorporates all of the elements mentioned in this section. Figure 3.24 shows diagram of the cross section of the damper, as well as how the vanes, and therefore the damping fluid, will move with the rotation of the rotor.

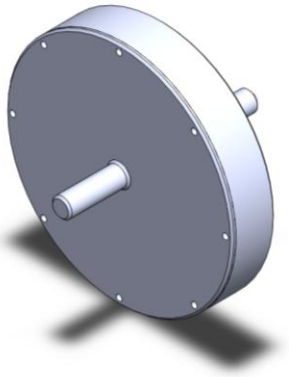

Figure 3.21: 3D CAD render of MCRVD

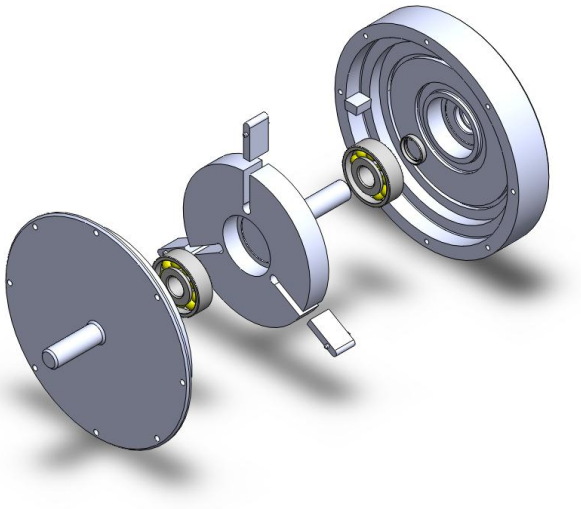

Figure 3.22: 3D CAD render of MCRVD components

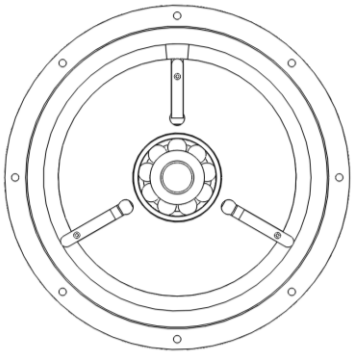

Figure 3.23: 3D CAD render of MCRVD (Top view; open stator)

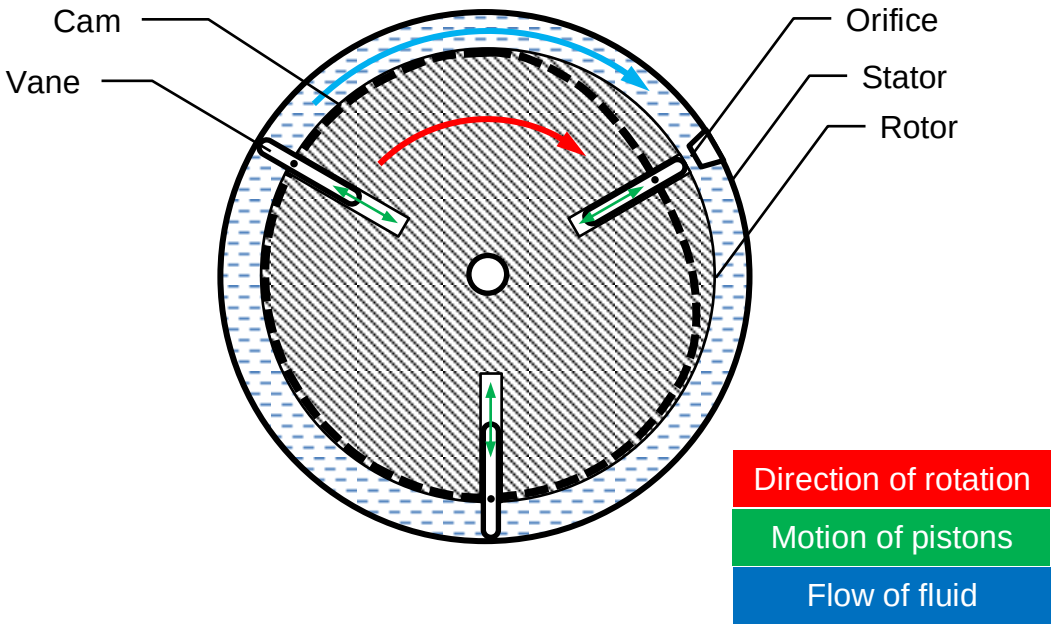

Figure 3.24: Diagram of MCRVD cross section

3.4.5 Testing and characterization of the MCRVD

Figure 3.25 shows the prototype damper mounted on a test rig. Testing and characterization of the MCRVD was carried out by Alt [2]. He had several observations:

- The damper produced a torque output that was relatively proportional to the input velocity [62].

- However, the damping coefficient was found to be very small, resulting in the output equation of the damper was dominated by non-linear terms (created as a result of friction in the system).
- The small damping coefficient also meant that large control outputs were required to correct for small torque deviations.

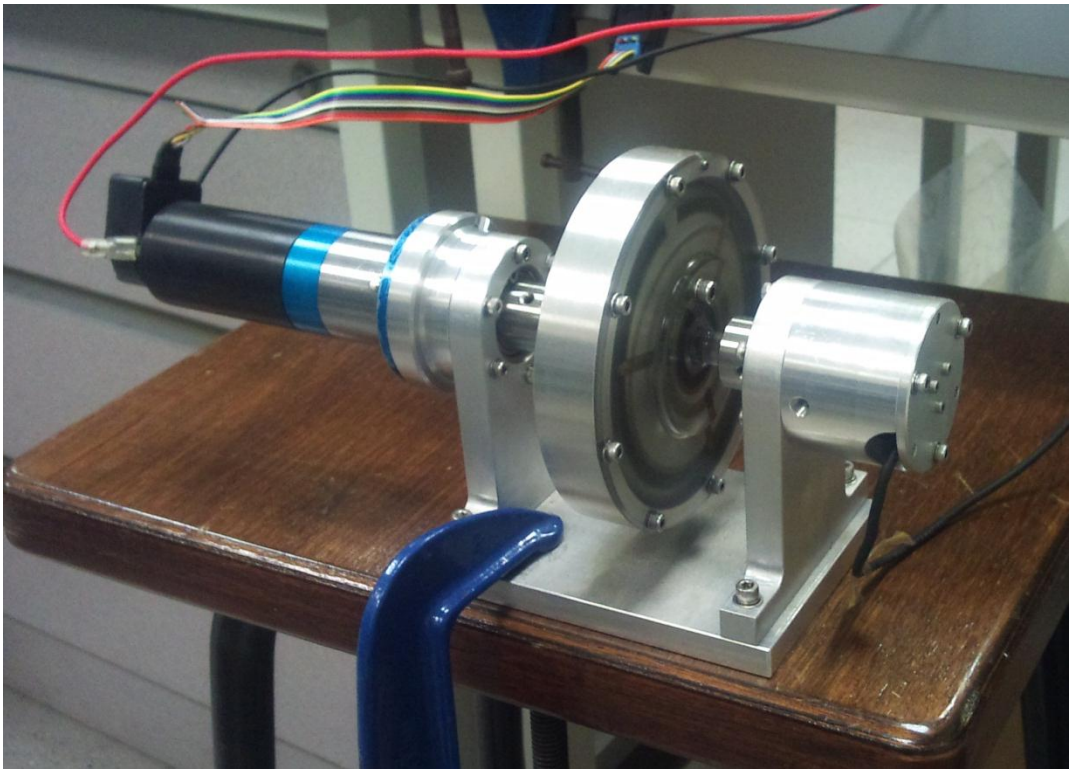

Figure 3.25: Picture of damper prototype mounted on test rig

Alt observed that there was periodic behaviour in the damper output, and was able to identify these components via Fast Fourier Transform. He was subsequently able to model the noise and use this model as feed forward.

Alt proposed several possible controllers for a complete actuator system employing the MCRVD. However, the physical implementations of these controllers were challenging due to the output force of the damper being very low, which would have made force

feedback difficult. However, he observed that an Exact State Linearization reduces the non-linear effects significantly, and that a state feedback controller with integral part can be used to control position and velocity of the motor and reject constant velocity disturbances. Alt also proposed design a new damper with a larger damping coefficient.

3.5 Continuous Rotary Piston Damper (CRPD)

As mentioned in the previous section, the main disadvantage of the MCRVD is that the damping coefficient was too small. A new design for a continuous rotary damper was proposed to overcome this problem. While the CRVD was based off the NCRD, this new damper was designed based on a radial piston pump/motor.

3.5.1 Radial piston pump/motor concept

In viscous dampers, the output force is generated from pressure in the damper fluid as it is forced through an orifice. Using the same concept, it is possible to implement a viscous damper simply by taking a hydraulic pump or motor, and connecting the inlets and outlets via a flow control valve; closing the flow valve would restrict the flow from the outlet to the inlet.

When the input shaft of the pump is turned, back pressure will be created at the compression chamber of the pump due to the resistance to fluid flow through the control valve. This back pressure would resist the input force to the shaft, thus creating the damping force.

A virtue of such a system is that the damping coefficient can be easily changed by controlling the flow valve between the outlet and inlet. However, as the damper has to be a self-contained device, it would be necessary to incorporate the valve into the pump.

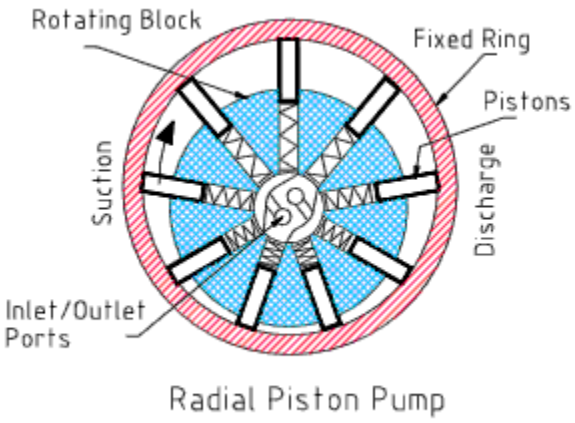

Figure 3.26: Diagram of a Radial Piston Pump

An ideal hydraulic pump/motor design to adapt from would be the radial piston pump, an example of which is shown in Figure 3.26. In this pump, the piston chambers are arranged in a radial orientation, with the inlet and output of the pump located at the centre of the rotor. As the rotor of the pump is turned, the pistons on the right forces fluid out of the pump via the outlet port, while the pistons on the left pulls fluid into the pump via the inlet port.

As mentioned earlier, the inlet and outlet ports of the pump could be connected via a flow control valve to create a damping effect. Two ways to implement this in the radial piston pump would be:

1. Replace the central inlet/outlet port section with a direct channel, in which an orifice can be implemented.

2. Replace the central inlet/outlet port section with a reservoir and seal off each piston chamber with an orifice, turning each separate piston chamber into a linear acting damper.

Method 2 was chosen for implementation due to sealing and fabrication considerations. A simplified diagram of the proposed damper is shown in Figure 3.27.

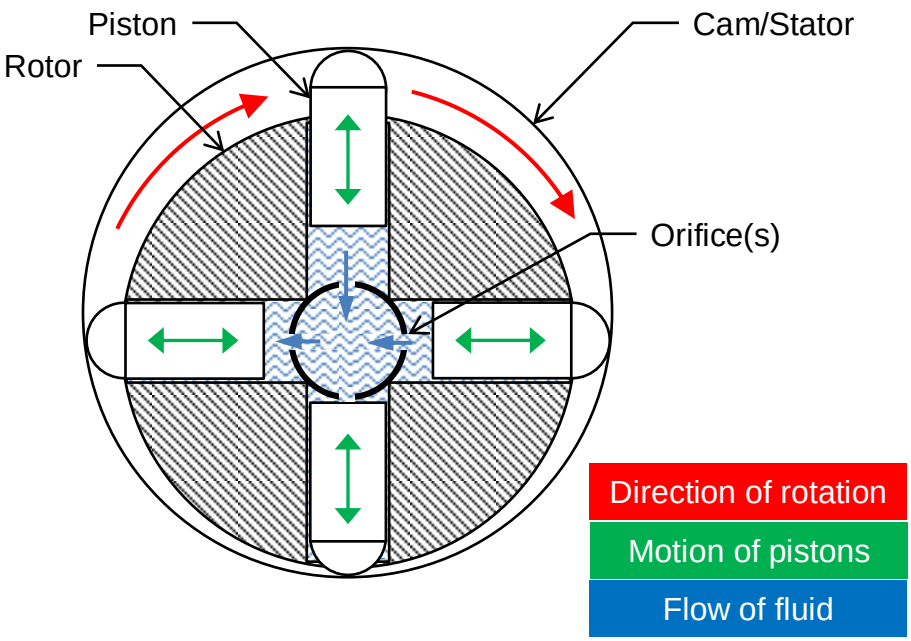

Figure 3.27: Continuous rotary viscous damper

3.5.2 CRPD design considerations

Drawing on experience gained from the design of the MCRVD, it decided that more attention was needed in the design of the cam for CRPD. Furthermore, it was decided to fabricate the CRPD to much tighter tolerances, albeit to higher cost. This section shares some insight into the design of the cam profile of the CRPD, as well as highlights some other design considerations that were taken.

Cam design considerations

In the MCRVD, the damping effect was generated from the fluid being pressurized between the moving vanes and the orifice; the pressurised fluid resists the movement of the vane, thus create a torque at the output shaft of the damper. However, in the MCRVD design, the interaction between the moving components resulted in oscillations in the output torque of the damper. This was caused by a changing pressure angle that the cam follower made with the cam groove as the rotor was turned. Alt was able to model these oscillations, and subsequent compensated for these oscillations using feedforward in his controller implementation [2].

In the case of the CRPD, the damping force is generated in the radially arranged linear acting pistons; the effective output torque is generated from the cam follower's interactions with the cam as the rotor is turned. As such, using the results from the CRVD, it can be predicted that output of the CRPD may also have oscillating components if the cam is not designed properly.

In simple radial piston pumps, a circular cam is commonly used. A quick analysis was done to see if a circular cam would be able to produce constant torque in the CRPD. Figure 3.28 below is a simple diagram of said damper. The outer circle represents the cam, while the inner circle represents a rotor with its axis offset from the axis of the cam.

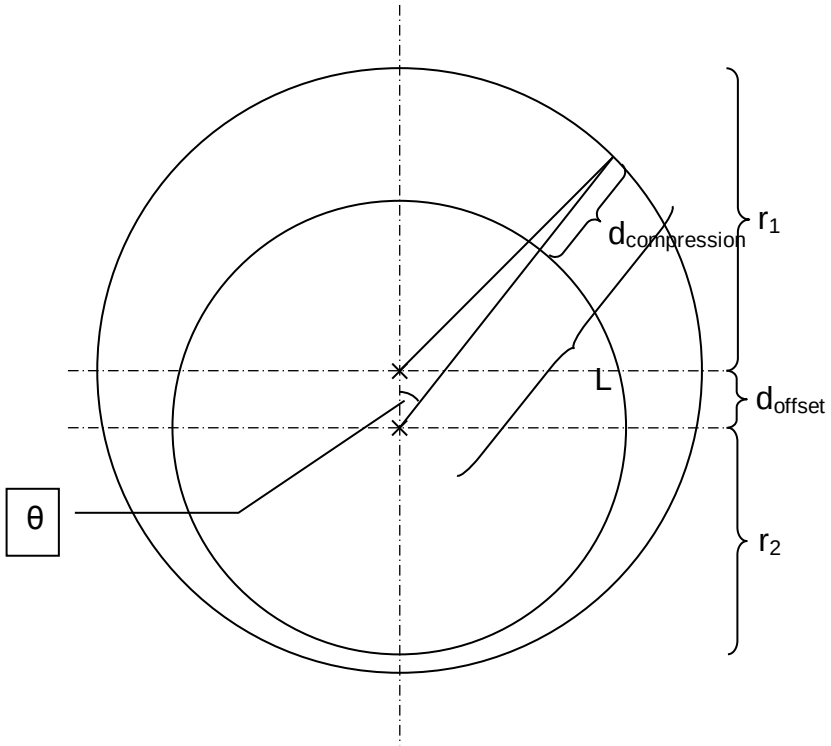

Figure 3.28: Analysis of a CRPD using a circular cam

For the above diagram, r_1 is the radius of the cam, r_2 is the radius of the rotor, d_{offset} is the offset distance between the axis of the cam and stator, and L denotes the distance from the cam surface to the axis of the rotor. An expression for L can therefore be found to be:

$$L = d_{offset} \cdot \cos\theta + \left({d_{offset}}^2 \cdot \cos^2\theta - {d_{offset}}^2 + {r_1}^2\right)^{\frac{1}{2}} \quad 3.4$$

Assuming the piston to behave as an ideal damper, an expression for the reaction force generated by the piston as the rotor is turned can be found to be:

$$F_{piston} = b \cdot \dot{d}_{compression} \quad 3.5$$

$$= b \cdot \frac{d}{dt}(L - r_2) \quad 3.6$$

$$= b \cdot \frac{dL}{dt} \tag{3.7}$$

$$= b \cdot \omega \cdot \left(-d_{offset} \cdot \sin\theta - \frac{{d_{offset}}^2 \cdot \cos\theta \cdot \sin\theta}{\left({d_{offset}}^2 \cos^2\theta - {d_{offset}}^2 + {r_1}^2\right)^{\frac{1}{2}}} \right) \tag{3.8}$$

Assuming that there are only normal forces (F_{norm}) acting at the point of interaction between cam and cam follower (ignoring friction), the force resisting the rotation of the rotor (F_r) can therefore be found from resolving the forces at the cam/cam follower interface.

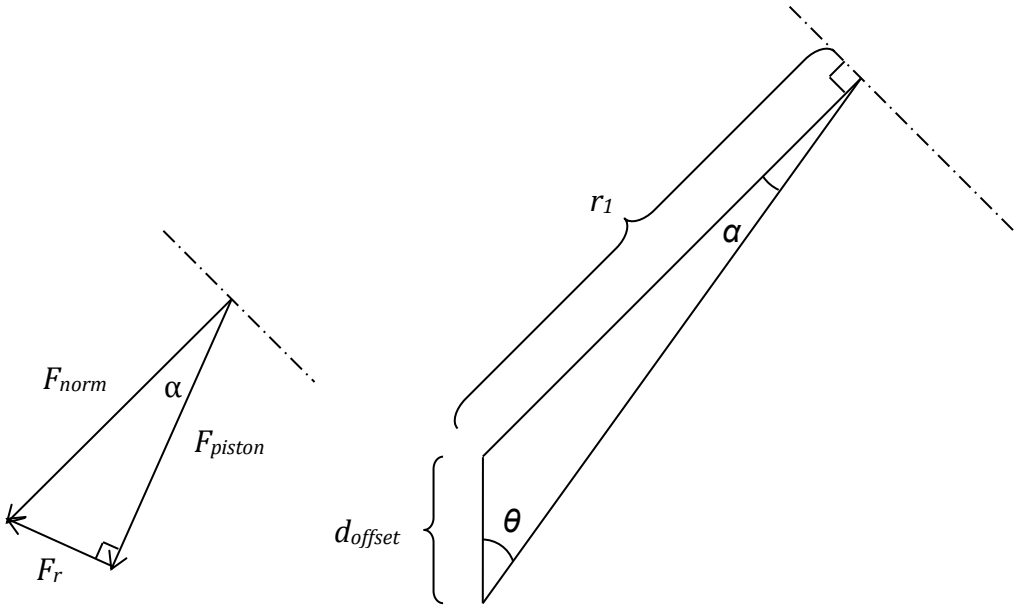

Figure 3.29: Force analysis at cam/cam follow interface

Thus the force resisting the rotation, F_r, can be found from the force triangle above to be:

$$F_r = F_{piston} \cdot \tan \alpha \qquad 3.9$$

where

$$\alpha = \sin^{-1}\left(\frac{d_{offset} \cdot \sin \theta}{r_1}\right) \qquad 3.10$$

The resistive torque, T_r, from one piston can be expressed as:

$$T_r = F_r \cdot L \qquad 3.11$$

Substituting equations 3.8 and 3.9 for F_r and L, an expression for T_r can be found. A plot of T_r against θ is shown below:

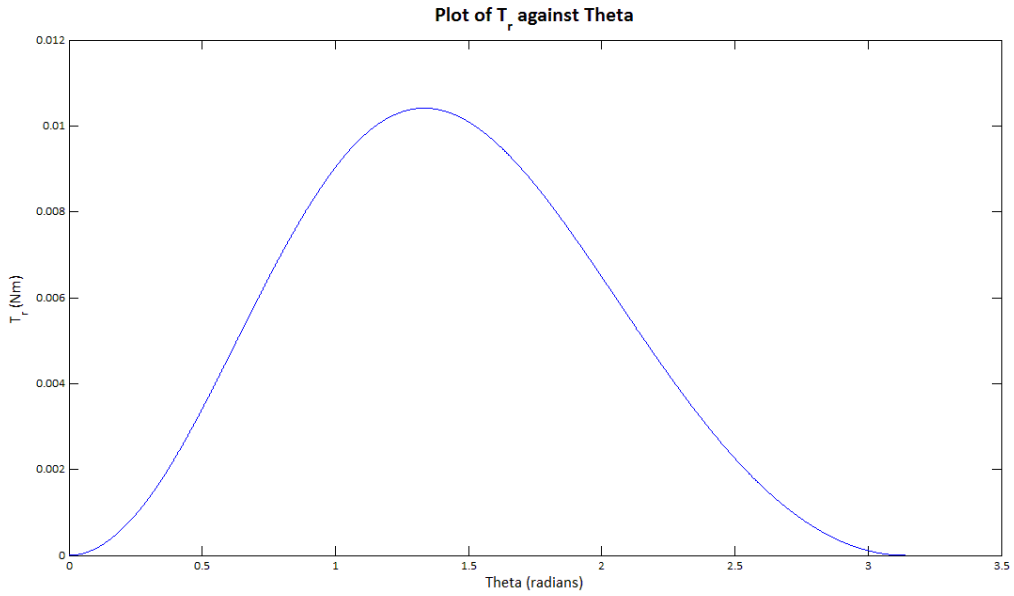

Figure 3.30: Plot of T_r against θ

The plot above is for a single piston. In the case of a 4 piston damper placed at 90° to each other, the output torque may be predicted to be as shown below:

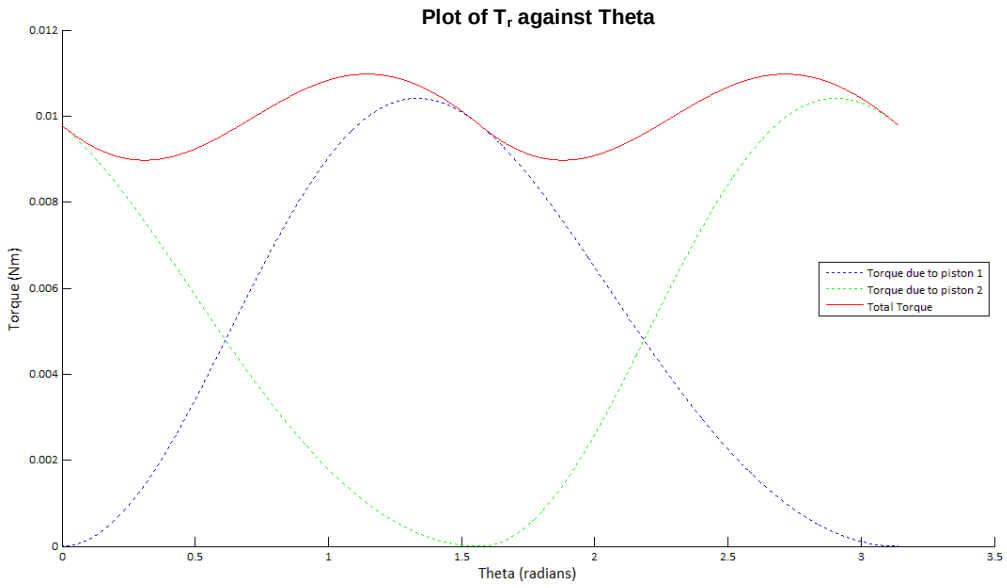

Figure 3.31: Plot of T_r against θ

As can be seen, the output torque is not constant, although the deviation in amplitude can be rather small depending on the parameters of the damper cam. The output of the damper can be "smoothened" further by implementing more pistons in the rotor. The fluctuations in output can also be compensated via a controller, just as Alt had done with the MCRVD.

Alternatively, a specific cam profile could be design to reduce these oscillations.

Generation of compensated cam profile

One way to obtain a constant total torque is to define the shape of the cam, rather than rely on a circular cam. To do this, a general expression for the torque must be obtained.

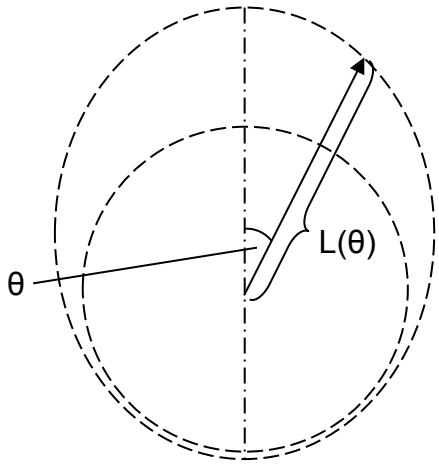

Figure 3.32: Simple drawing of cam and rotor

Just like before, L denotes the distance from the cam surface to the axis of the rotor (the smaller circle), and θ is the angle of the piston relative to the cam. However, L is defined some unknown function of θ; i.e. $L = f(\theta)$.

As before, it is assumed that the piston in the rotor behaves like a linear damper, i.e.:

$$F_{piston} = b \cdot \dot{x}_{compression} \quad (3.12)$$

$$= b \cdot \frac{d}{dt}(L(\theta) - r_{rotor}) \quad (3.13)$$

$$= b \cdot \frac{d}{dt} L(\theta) \quad (3.14)$$

$$= b \cdot \omega \cdot L'(\theta) \quad (3.15)$$

Next, it is necessary to find the resulting resistive force that opposes the stator motion. To do so, analysis of the cam gradient is necessary.

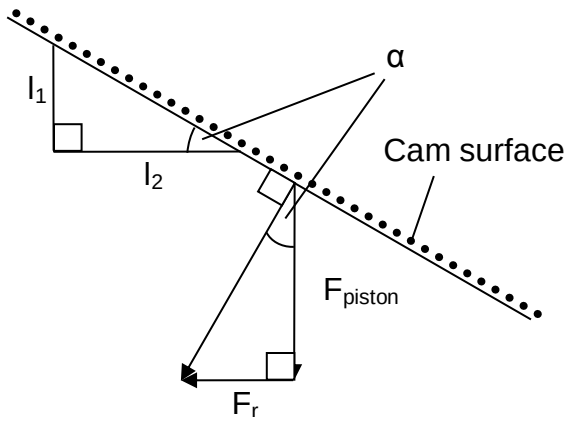

Figure 3.33: Analysis of force interaction at cam surface

Considering the two triangles above, it is clear that they are similar triangles. Therefore, the ratio of their sides should be the same, i.e. $\frac{F_r}{F_{piston}} = \frac{l_1}{l_2}$.

$$\frac{F_r}{F_{piston}} = \frac{l_1}{l_2} \quad 3.16$$

$$F_r = \frac{l_1}{l_2} \cdot F_{piston} \quad 3.17$$

However, since l_1/l_2 is effectively the gradient of the cam, then the above can be re-expressed as:

$$F_r = L'(\theta) \cdot F_{piston} \quad 3.18$$

Thus, the resistive torque would be:

$$T_r = F_r \cdot L(\theta) \quad 3.19$$

$$= b \cdot \omega \cdot L'(\theta) \cdot L'(\theta) \cdot L(\theta) \quad 3.20$$

$$T_r \quad = b \cdot \omega \cdot L'(\theta)^2 \cdot L(\theta) \tag{3.21}$$

By equating the above to some function for the desired torque output for a single piston, an O.D.E. can be obtained. Solving this O.D.E. would allow the appropriate cam to be found. For a four piston rotor, an ideal output would be in the form of $sin^2\theta$ as shown below.

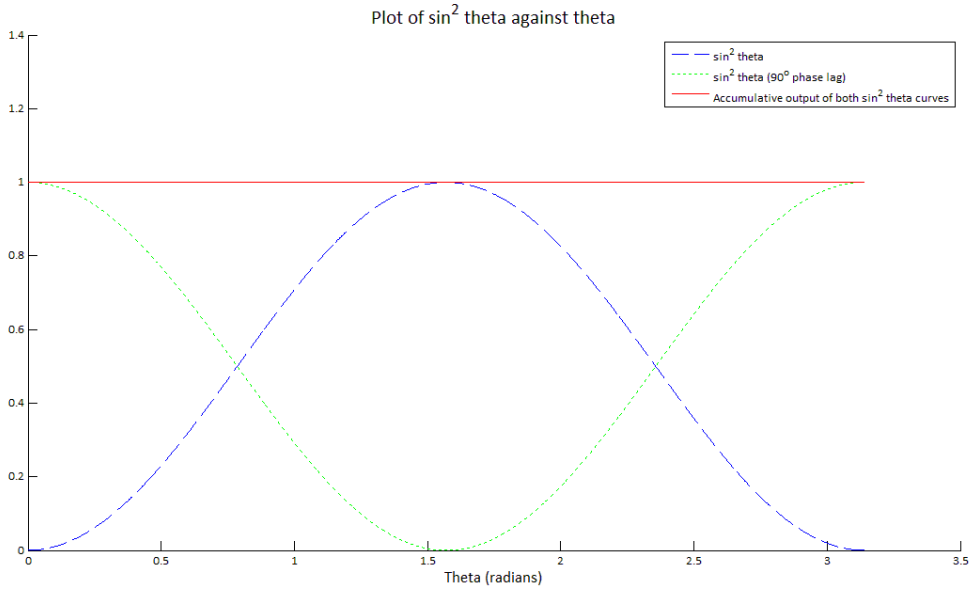

Figure 3.34: Plot of $sin^2\theta$ against θ

Therefore, the O.D.E to solve is:

$$L'(\theta)^2 \cdot L(\theta) \quad = \mathrm{K} \cdot \sin^2 \theta \tag{3.22}$$

Using Matlab, a solution for *L(θ)* is:

$$L(\theta) = \left[\frac{1}{2}k_1 + \frac{1}{2}k_2 cos\theta\right]^{\frac{2}{3}} \quad (3.23)$$

where

$$k_1 = r_{outer}^{\frac{3}{2}} + r_{inner}^{\frac{3}{2}} \quad (3.24)$$

$$k_2 = r_{outer}^{\frac{3}{2}} - r_{inner}^{\frac{3}{2}} \quad (3.25)$$

Thus, the expression for the resistive torque for one piston would be:

$$T_r = b \cdot \omega \cdot K \cdot \sin^2\theta \quad (3.26)$$

where

$$K = \frac{2}{9}\left(r_{outer}^{\frac{3}{2}} - r_{inner}^{\frac{3}{2}}\right)^2 \quad (3.27)$$

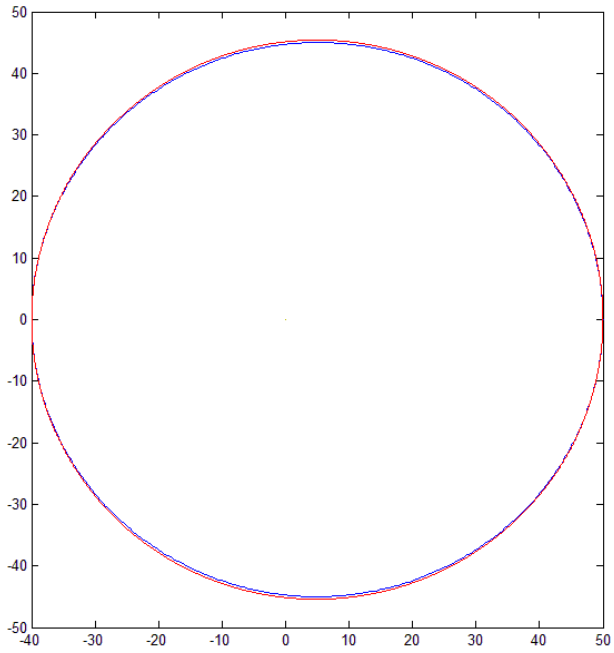

Figure 3.35: Plot of cam calculated as defined by equation 3.23

Figure 3.35 above is a plot of the proposed cam (in red); a circle of radius 45 mm (in blue) was plotted on the same axis for purpose of comparison. Considering that the fluctuations for a circular cam are rather small, it is predictable that the compensated cam does not differ much from the circular cam.

Other design considerations

Friction: In order to reduce the friction between the cam follower and cam surface, cam rollers were implemented in the final design. Roller bearings were also used to ensure concentricity between the rotor and stator, and prevent any contact between the two components.

Sealing: Piston seals were used to ensure minimal leakage of damping fluid from the piston chambers. To reduce friction between the piston and chamber walls, nylon piston guide stripes were also incorporated into the final design.

Orifice: An attempt was made to incorporate an orifice with an adjustable opening. However, as this orifice was not very effective at varying the damping coefficient, the design was modified to use interchangeable plates of various orifice sizes.

3.5.3 Final design for the CRPD

Figure 3.36 and Figure 3.37 are CAD renders of the final CRPD designs; the former is of the damper when it is completely assembled, and the latter is an exploded view for an overview of the various components of the damper. Figure 3.38 is a top view of the open damper. The actual prototype, as pictured in Figure 3.39, was fabricated out of 6061aluminum (rotor and stator) and stainless steel (pistons).

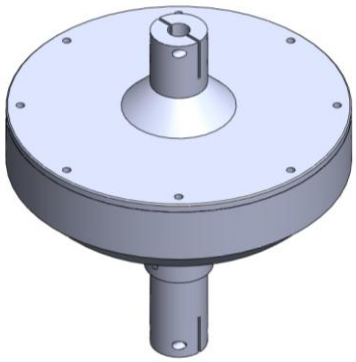

Figure 3.36: 3D CAD render of CRPD

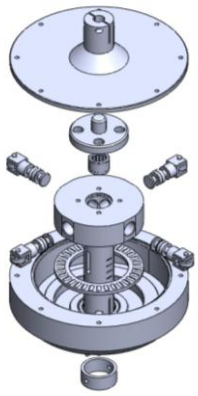

Figure 3.37: 3D CAD render of CRPD components

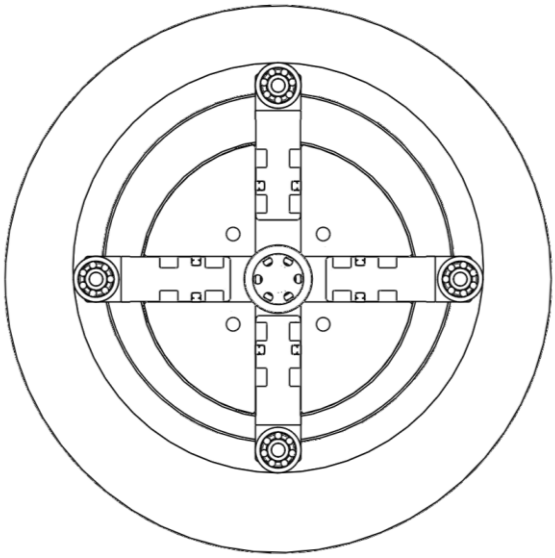

Figure 3.38: CAD render of CRPD (Top view; open stator)

Figure 3.39: Picture of CRPD prototype

3.6 Summary

This chapter provided an account into the design of two rotary dampers, the MCRVD and CRPD; both of which were intended to be used in the implementation of an SDA.

The MCRVD was designed to be an improvement over Chang's CRVD. While the design was more successful in that it did not experience any jamming and was able to provide linear viscous damping, the damping coefficient was very small. There were also some non-linear oscillations in the damper output torque due to the friction interaction in the cam system.

The CRPD was designed to overcome the shortfalls of the CRVD, and took a different design approach of adapting a radial piston pump to achieve the damping effect. Testing and characterization of the CRPD is further elaborated in the next chapter.

It can be seen that design is a reiterative process, which requires several cycles of design, testing, and then further improvement until an ideal outcome is achieved. Greater detail was provided in this chapter with the goal that it could aid future work on continuous rotary dampers.

Chapter 4 - Identification of damping behavior in the CRPD

This chapter will present the results of test ran on the CRPD presented in the previous chapter, as well as present work done to identify the damping behaviour of the CRPD

4.1 Experimental setup

Figure 4.1 below shows a diagram of the complete setup of the proposed Series Damper Actuator. The output of a brushed DC motor is directly connected to the input of a damper. The velocity output of the DC motor is measured via an encoder mounted directly on the DC motor fed to a motor driver embedded in a controller. The output force of the damper is recorded by a force/torque sensor connected to a DAQ module embedded on the same controller as the motor driver. The controller acts as the interface between the hardware and the computer.

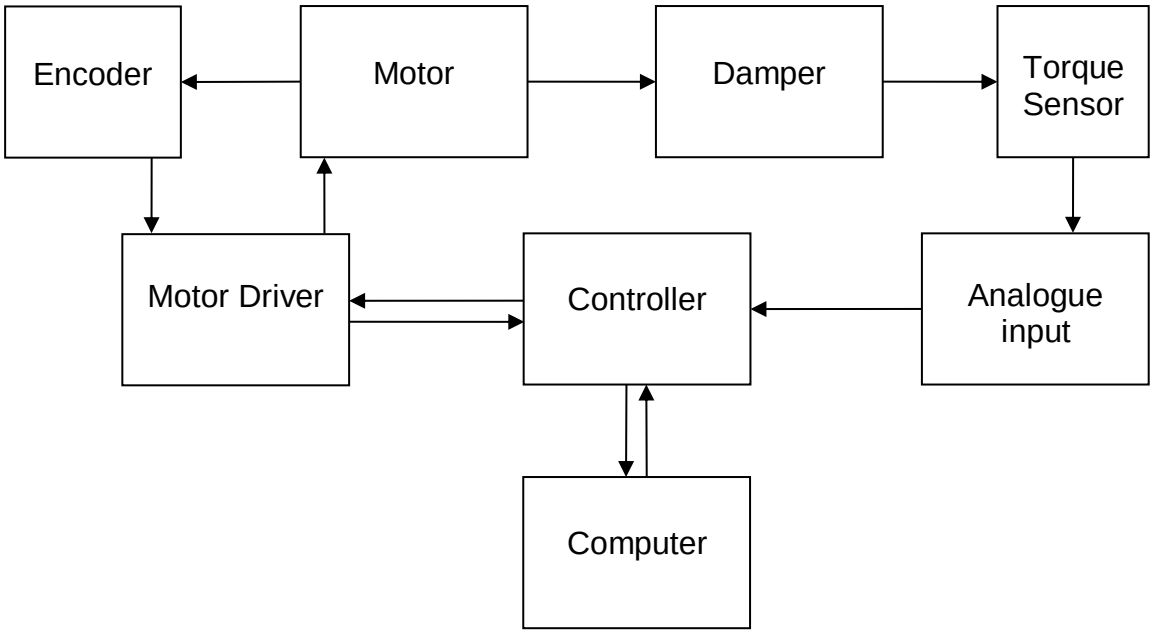

Figure 4.1: SDA setup

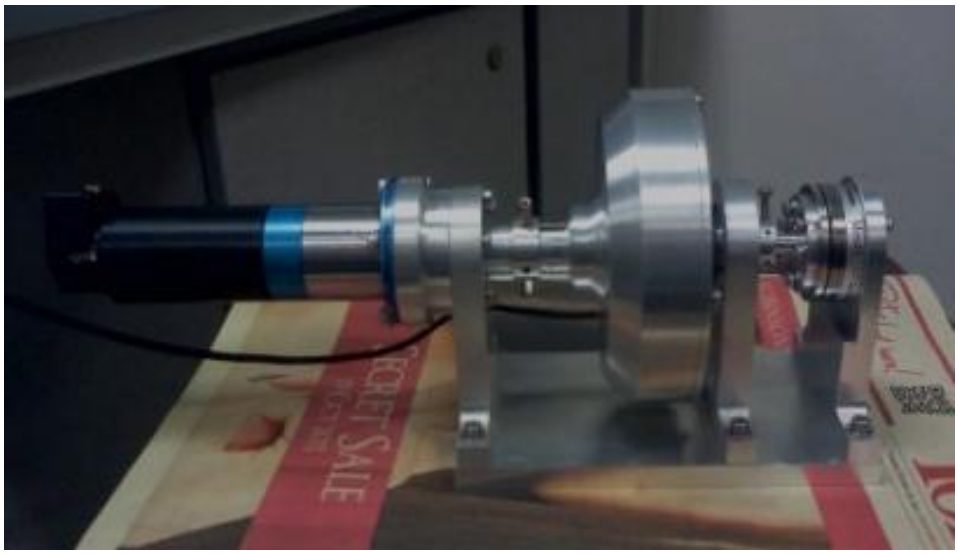

Figure 4.2: Picture of the CRPD mounted on the test rig

Motor

The employed motor is a brushed DC permanent magnet motor (3863A024C, Faulhaber) with a planetary gear. The gear ratio is given with r = 134:1.

Rotor inertia (J_m = 110gcm), nominal voltage (U_{nom} = 24V), input and output limits, such as maximum current (I_{max} = 3:8A), maximum output torque (T_{max} = 110mNm), maximum speed (v_{max} = 8000rpm) and maximum output power (P_{max} = 220W) are provided from the manufacturer.

Encoder

The encoder employed is an optical incremental encoder (HEDS-5540-S12, Avago) mounted directly to the main shaft of the DC motor.

The incremental encoder has a resolution of 400 counts per revolution, since it employs two quadrature outputs, which sense 100 pulses per revolution. Therefore a sufficiently

accurate position and velocity signal can be measured. Digital output signals are sent to the motor driver.

Motor Driver

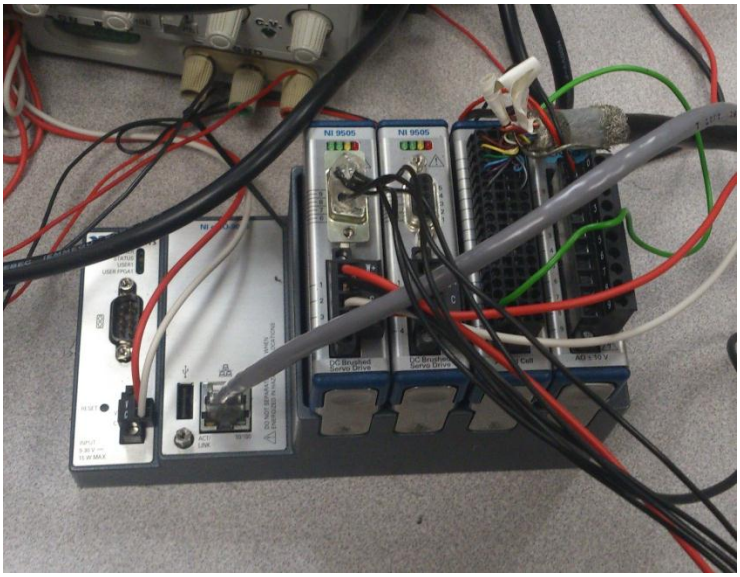

Figure 4.3: Picture of compactRio and mounted modules

The employed motor driver is a full H bridge brushed DC servo drive module (NI9505, National Instruments) mounted onto a real-time controller (NI cRIO-9076, National Instruments) as pictured in Figure 4.3. It receives the encoder signal and delivers the control input to the motor in the form of pulse-width modulation.

The controller that the motor driver is mounted onto serves to decode and the encoder signal, as well as implement the motion control. The code to do this is designed on a computer, and then executed by a field-programmable gate array circuit on the controller.

Input and output limits, like maximum voltage ($V_{max,driver}$ = 30V), maximum continuous power output ($P_{max,driver}$ = 150W) and maximum continuous current ($I_{max,driver}$ = 5A) are

provided from the manufacturer. The limit values of the driver are above the ones of the motor and therefore do not restrict the system.

Force/Torque Sensor

Figure 4.4: Picture of ATI mini45 F/T transducer [63]

The force/torque sensor employed to measure the output torque of the damper is a multi-axis force/torque measurement system (mini45 F/T sensor SI-580-20, ATI). The sensor system consists of a transducer, interface electronics and cabling.

The transducer uses a setup of silicon strain gauges to sense forces. It measures force and torque along and about all three axes. For a strain gauge the signal to noise ratio is comparably low. The interface electronics convert the force/torque readings from analogue to digital, which are then read via the DAQ PCI card mounted onto the PC.

The signal from measurement system can be read directly; or with the aid of an appropriate calibration matrix, the actual force/torque readings can be calculated. This is done through proprietary software provided by the sensor manufacturer (ATI Industrial Automation, ATIDAQFT.NET.MSI).

Computer

The computer serves as the user interface, enabling the user to communicate with the system. In addition to presenting information recorded from the system, it also allows the implementation of motion, and subsequently force control through software.

For this setup, the computer serves as the “host” and communicates with the Ni compactRio via fast Ethernet. Programming of the NI compactRio on board FPGA is done through NI’s proprietary Labview software. The FPGA is responsible for acquiring information via its I/O and motor driver modules, executing the velocity and current control loop, and generating the pulse-width modulation for the motor driver output.

LabView is a graphical programming environment, which can be used to measure, test and control systems. It is perfectly suitable for visualizing data and establishing a user interface. Moreover it allows an effective and fast programming due to its graphical programming concept.

Labview is used to visualize the measured data of both encoder and torque sensor. Furthermore the force control is realized with the help of LabView.

Damper

The damper used is a prototype fabricated based on the CRPD design as presented in Section 3.5 of Chapter 3.

4.2 Considered Signals

4.2.1 Input and output signal

The rotary damper is directly connected to the output shaft of the motor, which rotates at a circular velocity $\dot{\theta}_s(t)$. Its angular displacement is given by the time dependent function $\theta_s(t)$.

In this thesis position and speed of the motor are seen as input signals. In order to prevent confusion and inconsistency in discrete considerations shaft position and velocity are respectively renamed to $p(t)$ and $v(t)$ for continuous signals and $\underline{p}$ and $\underline{v}$ for discrete time dependent signal vectors.

The output of the system is the resulting torque, which is measured by a torque sensor. Only the damper system is analysed in this chapter. That is why the motor dynamics are neglected and it is assumed that it is possible to send a desired velocity signal to the damper.

In order to obtain torque outputs for specific desired velocity signals, a velocity control for the motor is employed. The controller is implemented and tuned by using National Instruments Labview software and compactRio.

4.2.2 Discrete and continuous signals

In this thesis, the considered signals are treated as both discrete vectors and time based continuous functions. Analysis and processing of the considered signals was done via a discrete approach; however, a continuous treatment was necessary to make system-theoretical considerations more convenient.

The constant sampling period for the discrete position, velocity and torque is $\Delta t = 0.025s$. The j[th] entry of the discrete time vector $\underline{t}$ with $j = 1(1)N$ and $N = 1024$ is given by

$$t_j := \underline{t}(j) = (j-1) \cdot \Delta t \qquad 4.1$$

Further calculations are based on discrete velocity input vector $\underline{v}_i$ with a constant value v_i. The index $i = 1(1)17$ indicates the considered value of the shaft speed. The measured input values are shown in **Table 1** below.

Table 1: Considered velocities for damping identification

Velocity Index	**Value (motor velocity in rpm)**
1	300
2	400
3	500
4	600
5	700
6	800
7	900
8	1000
9	1500
10	2000
11	2500
12	3000
13	3500
14	4000
15	4500
16	5000
17	5500

The expression for the velocity is

$$v_{ji} := \underline{v}_i(j) = v_i(t_j) = v_i \qquad 4.2$$

The corresponding discrete torque output vector signal $\underline{T_i}$ of a certain velocity vector $\underline{v_i}$ consists of the following entries:

$$T_{ji} = \underline{T_i}(j) = T_i(t_j) \tag{4.3}$$

If the considered signals are interpreted as continuous function, the velocity signal $v(t)$, the torque $T(t)$ and the position signal $p(t)$ are differentiable functions of time.

4.3 Test Procedures

The damper was tested at several speed input settings and with a variety of orifice sizes. The motor was set to output a constant speed, and the resultant output torque was recorded. While the original damper design incorporated an orifice of variable cross-sectional area, the final test setup used interchangeable orifices to further reduce internal leakages.

Below is a table listing the various settings used:

Table 2: Settings used in the experiments

Speed inputs ($rads^{-1}$)
31.4
41.9
52.4
62.8
73.3
83.8
94.2
104.7
157.1
209.4
261.8
314.2
366.5
418.9
471.2
523.6
576.0

Available orifice sizes (hole diameter, mm)
10 (100% open)
7 (49% open)
5 (25% open)
3 (9% open)
1 (1% open)

The damper was tested on each orifice setting, at input velocities as shown in the table above. Below is a sample plot of the damper output toque against the input angular velocity for different orifice settings.

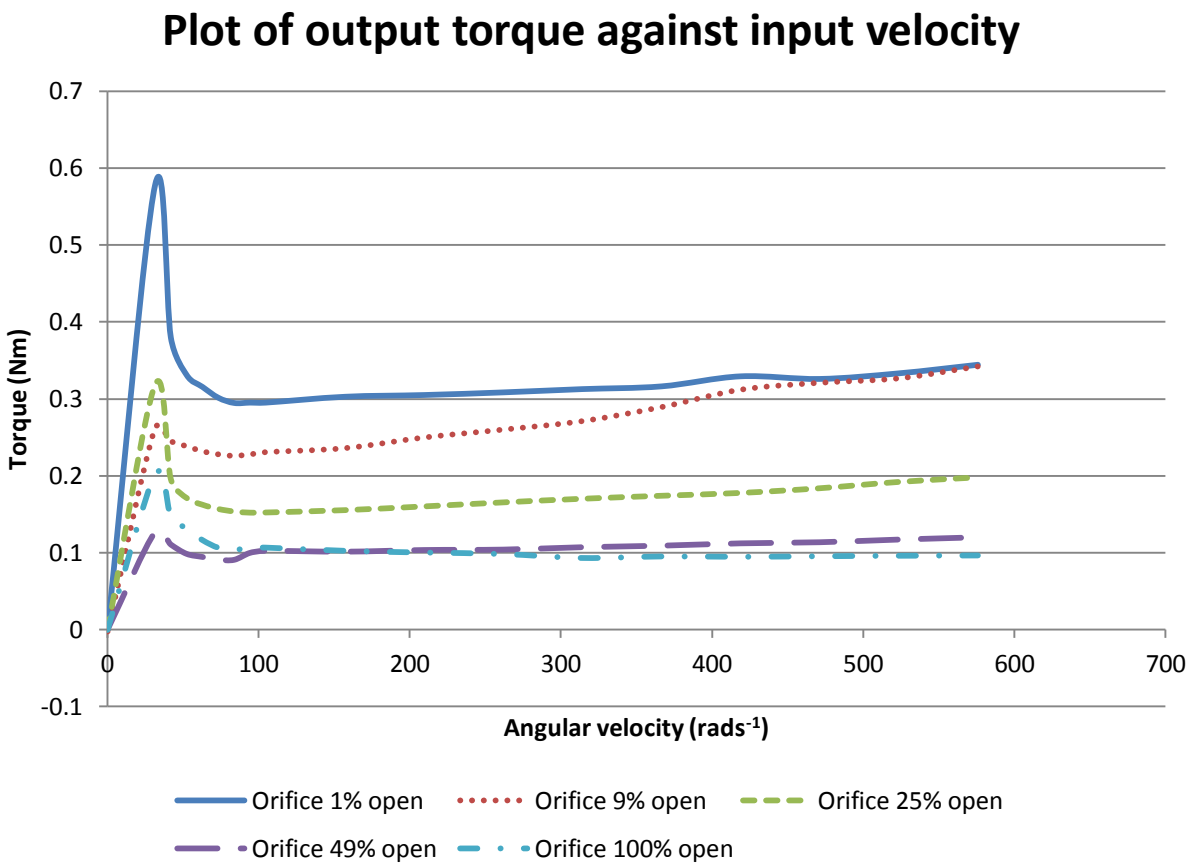

Figure 4.5: Plot of output torque against input velocity

From the plot in Figure 4.5, it can be seen that torque output displays some initial spike in torque, before increasing proportionally starting from angular velocities of 100 rads^{-1}. The gradients of each curve generally increases with a decrease in orifice size; this is in line will expectations that decreasing the orifice size will increase the damping effect. The exception to this trend is when the smallest orifice size of diameter 1 mm is used; the torque increases less quickly with velocity as compared to a 3 mm diameter orifice. Possible reasons for this will be discussed later.

In his analysis of the CRVD, Alt was successful at creating a model that could accurately describe the damper behaviour. He was also successful at designing a

controller that managed to improve the output torque performance, primarily by reducing the periodic fluctuations caused by friction in the damper. Considering his success with the CRVD, it was decided the similar approach be adopted in the analysis of the CRPD. The analysis of the damper behaviour involved identifying parameters for the non-periodic and periodic parts of the damper, with the initial goal of using the model to implement a controller.

4.4 Identification of parameters of non-periodic components

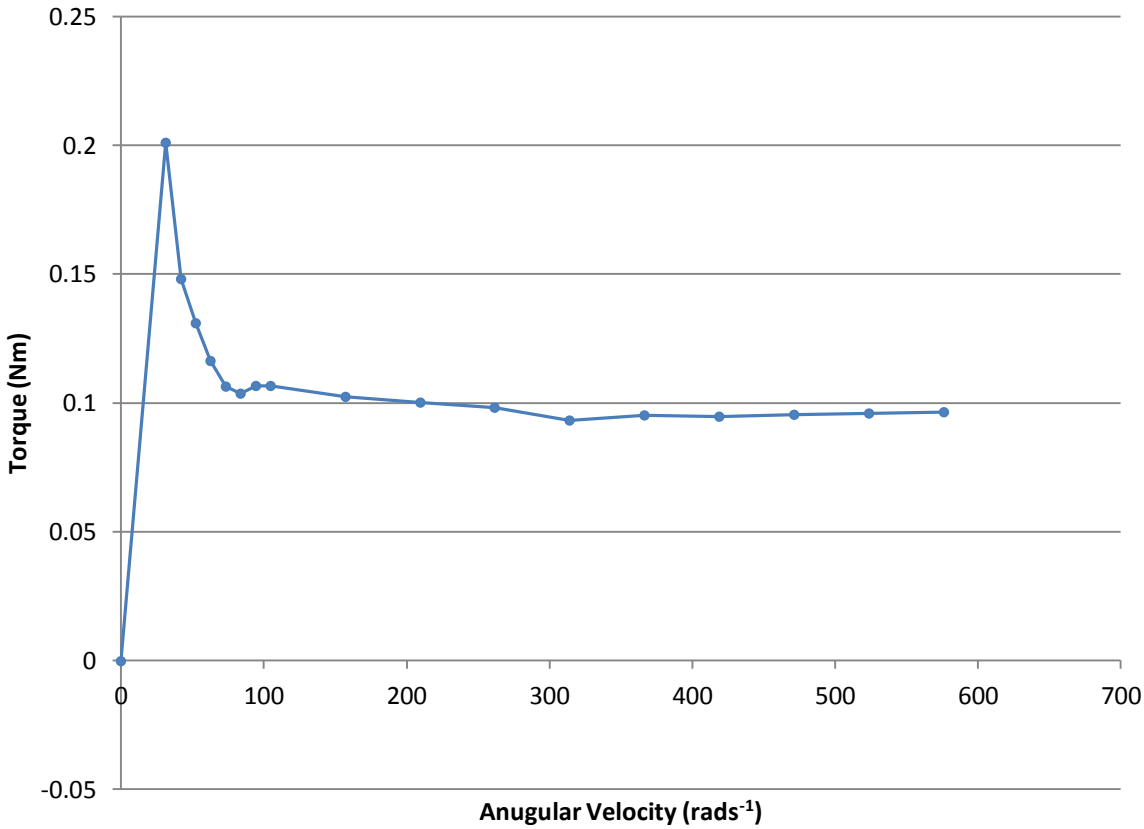

Figure 4.6: Plot of torque against velocity for an orifice size of diameter 10 mm

In order to model the effects of stiction and coulomb friction, we consider the damper without any viscous damping due to the hydraulic fluid.

Above in Figure 4.6 is the plot for the open orifice. In this configuration, the piston chambers are completely uncovered, allowing free flow of fluid in and out of the chamber. As such, there should be no damping effect due to the hydraulic fluid, and the torque generated here should be due to the stiction between the piston and its chamber, as well as dynamic friction in the bearings that were used as cam followers.

The expression that was used to describe the curve was

$$T_0 = c_1\big(v(t)\big)^{c_2} + c_3\big(v(t)\big) + c_4 \qquad 4.4$$

where the first term describes the stiction and coulomb friction, and the second term describes the viscous damping due to the hydraulic fluid. Using the curve fitting toolbox in Matlab, c_1, c_2 and c_3 can be found to be 564.4, -2.5, -8.05×10^{-6} and 0.09924 for a 100% opened orifice. By analysing the other torque outputs for different orifice settings, similar coefficients can be found for the other orifice settings as shown in **Table 3** below.

Table 3: Parameters for expression describing the torque/velocity relationship

Orifice setting, O_p	100% open	49% open	25% open	9% open	1% open
C_1	564.4	195.7	970.4	318.4	1636
C_2	-2.5	-2.5	-2.5	-2.5	-2.5
C_3	-8.05E-06	5.59E-05	0.0001289	0.0002417	0.0001575
C_4	0.09924	0.08859	0.1258	0.2021	0.2577

Based on the experimental data, generalised polynomial expressions could be used to relate the individual coefficient values and the orifice settings. The derived expression is:

$$\begin{bmatrix} c_1 \\ c_2 \\ c_3 \\ c_4 \end{bmatrix} = \begin{bmatrix} 0 & 0.2255 & -33.6 & 1669 \\ 0 & 0 & 0 & -2.5 \\ -8.372 \times 10^{-10} & 1.699 \times 10^{-7} & -1.204 \times 10^{-5} & 3.369 \times 10^{-4} \\ -5.774 \times 10^{-7} & 1.245 \times 10^{-4} & -8.35 \times 10^{-3} & 0.2665 \end{bmatrix} . \begin{bmatrix} o_p^3 \\ o_p^2 \\ o_p^1 \\ o_p^0 \end{bmatrix} \quad 4.5$$

The coefficients were obtained using the curve fitting toolbox in Matlab software.

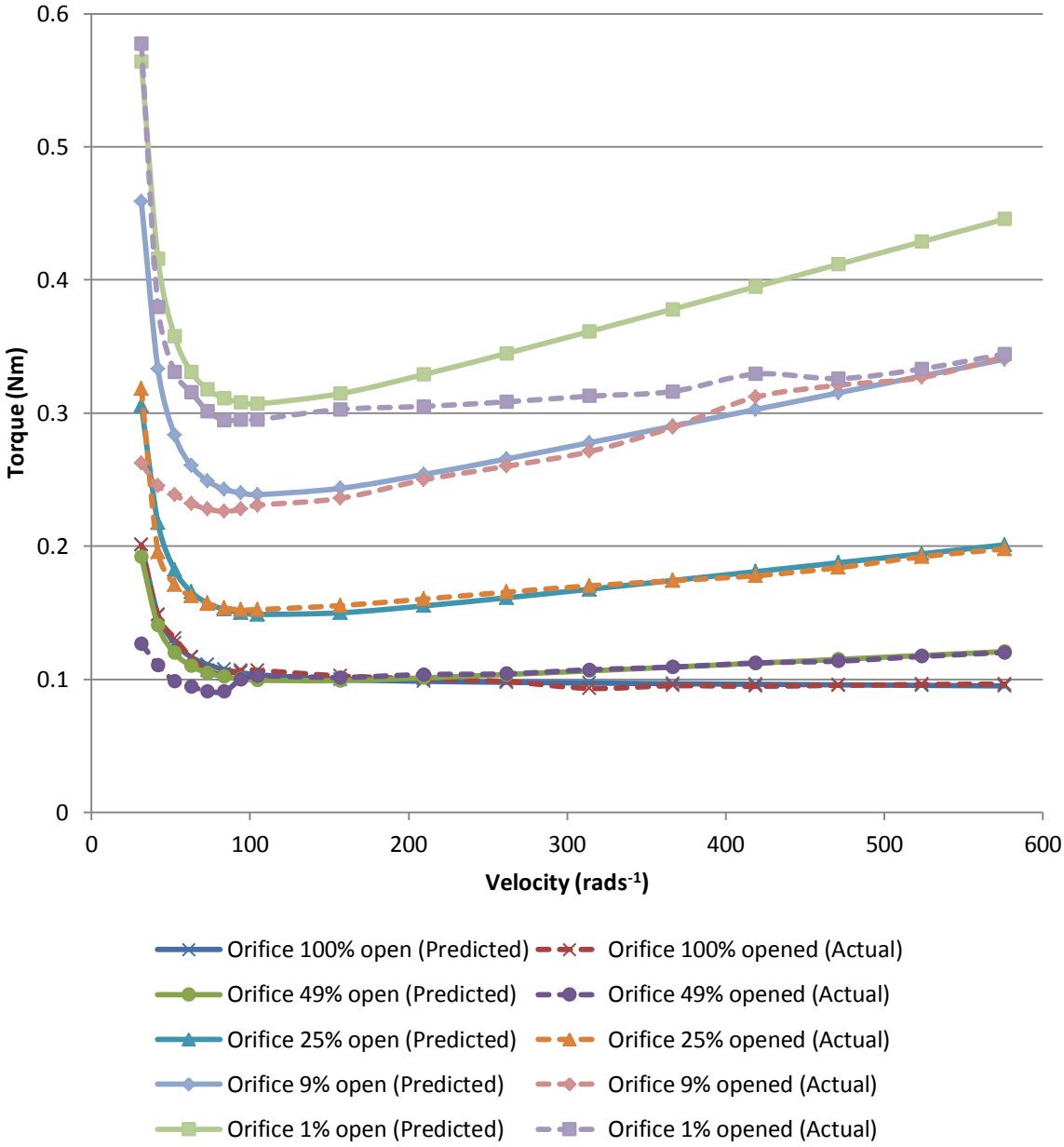

Figure 4.7: Comparison of model output against experimental results

The plot shown in Figure 4.8 compares the output predicted by the model and the experimental data. It can be seen that the model is reasonably able to predict the output torque of the damper at angular velocities of 100 rads^{-1} and above, with the exception of the orifice setting of 1% open. However, at velocities below 100 rads^{-1}, the behaviour of the torque output becomes difficult to predict accurately.

Considering that it may be hard to predict the behaviour at low speeds, as well as challenges at controlling the motor output at low speeds due to the resolution of the encoder, it may make more sense to model the behaviour of the damper for velocities higher than 100 rads^{-1}; considering that the orifice setting also affects the torque output, it may be possible to use the orifice setting as a force input as well.

Following a similar method as before, the non-periodic portion of the damper output can be given by the following expression:

$$T_{np}(v, o_p) =$$

$$\begin{bmatrix} v^1 & v^0 \end{bmatrix} \cdot \begin{bmatrix} -1.964 \times 10^{-9} & 3.554 \times 10^{-7} & -2.015 \times 10^{-5} & 4.065 \times 10^{-4} \\ -5.768 \times 10^{-6} & 5.139 \times 10^{-4} & -1.156 \times 10^{-2} & 2.999 \times 10^{-1} \end{bmatrix} \cdot \begin{bmatrix} o_p^3 \\ o_p^2 \\ o_p^1 \\ o_p^0 \end{bmatrix} \quad \text{4.6}$$

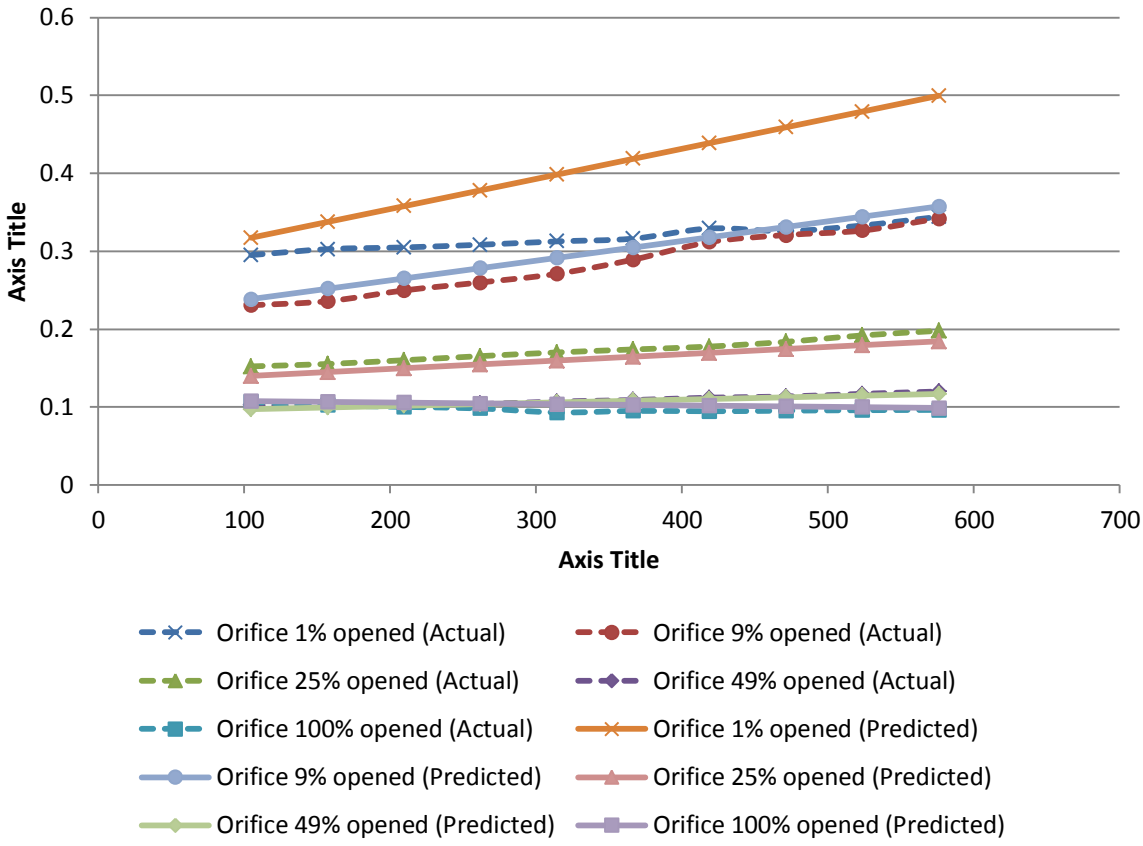

Figure 4.8: Comparison of model output against experimental data

As before, the expression is capable of predicting the output of the damper for orifice settings of 100%, 49%, 25% and 9% opened. However, it is similarly unable to predict the output torque for an orifice setting of 1% open. Considering that several trials were run to similar effect, it is possible that damper output for an orifice setting of 1% and 49% does indeed consistently converge towards 0.357 Nm with increasing velocity. If so, then an orifice setting of 1% may well be redundant for this particular setting, although modifications to the orifice section may well remedy this problem.

4.5 Identification of parameters of periodic components

In Alt's analysis of the CRVD, he was successful in identifying the parameters for the periodic part of the signal by using an expression that describes the periodic part as a combination of sine waves. Here an attempt was made to do the same.

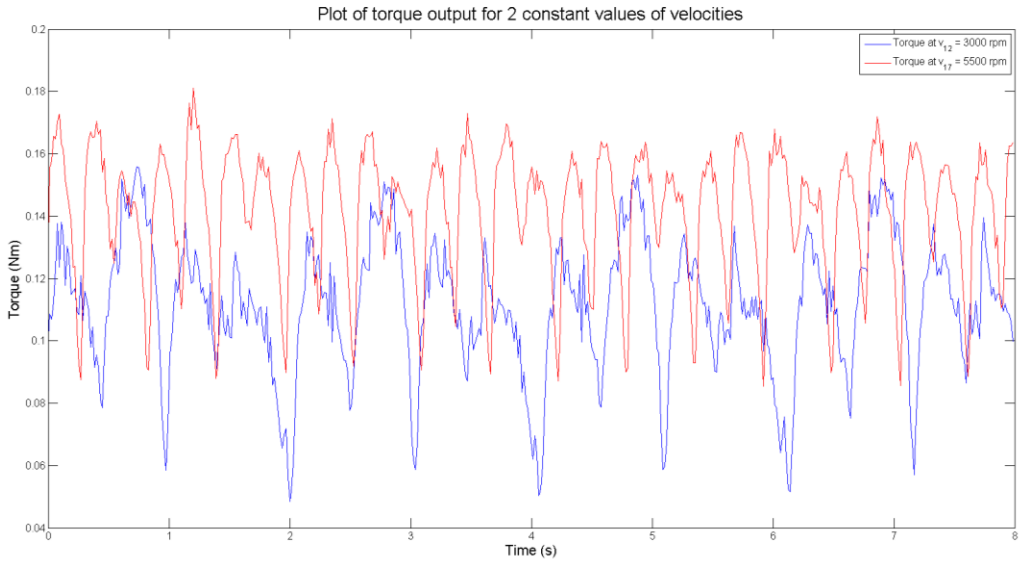

Figure 4.9: Torque output for 2 constant values of input velocities

Figure 4.9 above shows sample torque outputs for 2 different velocity inputs. It can be seen that both the mean value of the torque output and the non-linear part of the torque signal changes with the velocity input. The periodic behaviour is likely to be caused by position dependant friction.

The following figures are of 3 torque signals, corresponding to the different velocities outputs of 1000 rpm, 3000 rpm and 5000 rpm, plotted in the frequency domain. These plots were obtained through executing Fast Fourier Transform on the torque signals to transform them form the time domain to the frequency domain. This was accomplished in Matlab using the 'fft' command, which implements a Fast Fourier Radix 2 Algorithm.

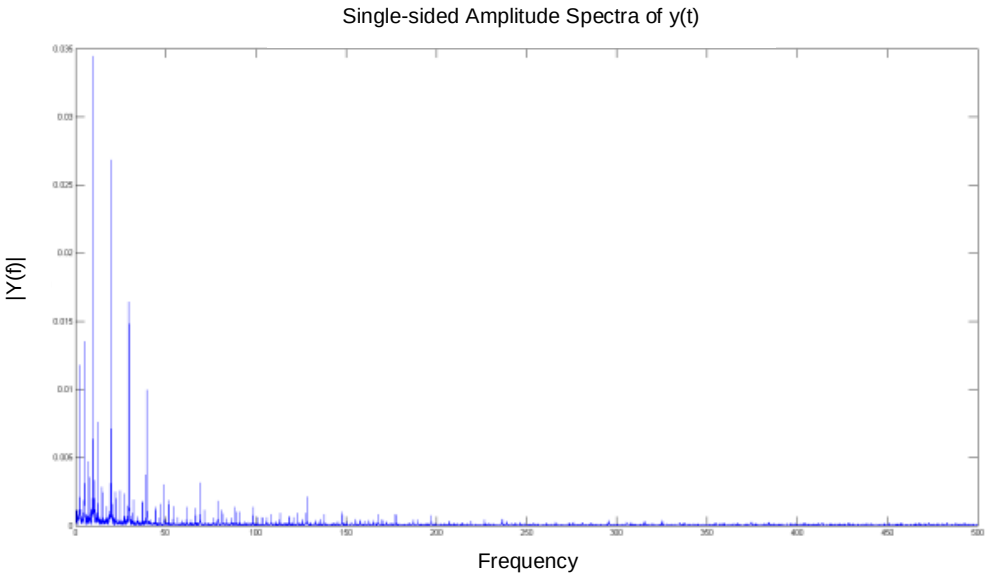

Figure 4.10: One-sided amplitude spectra for an input velocity of 1000 rpm

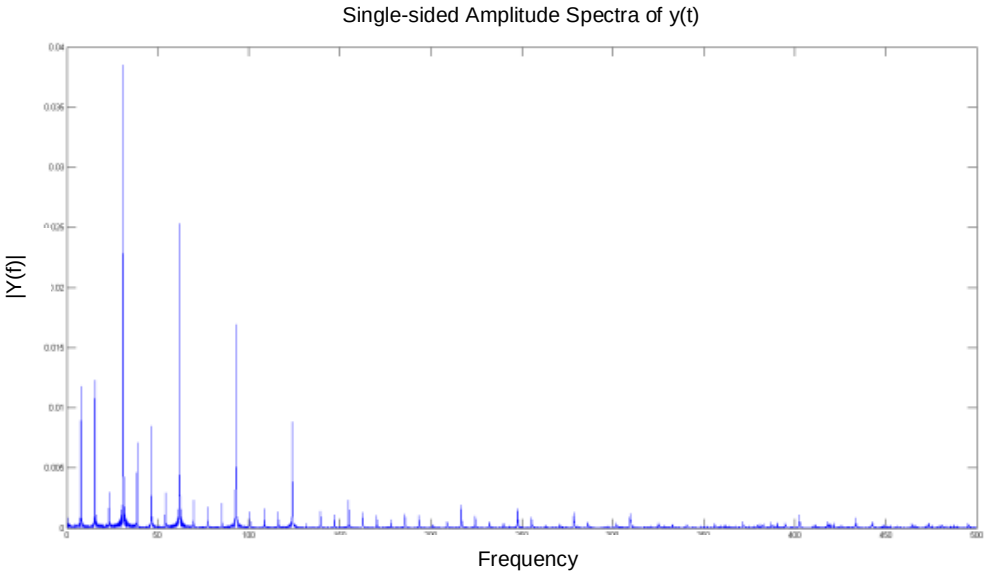

Figure 4.11: One-sided amplitude spectra for an input velocity of 3000 rpm

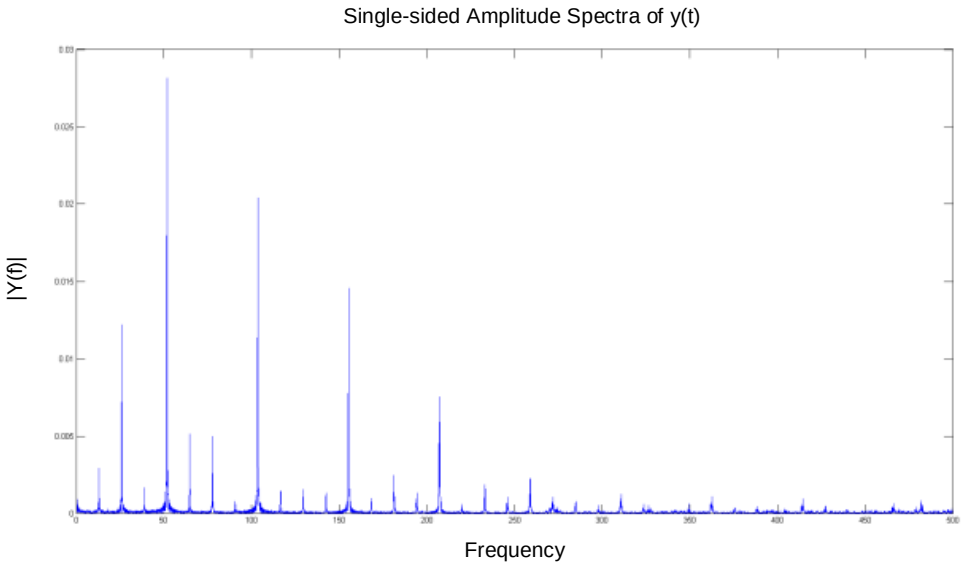

Figure 4.12: One-sided amplitude spectra for an input velocity of 5000 rpm

Through the frequency domain, the aim is to find a model for the periodic part of the torque signal by predicting the frequencies, amplitudes and phases of the five sine waves for every velocity. This information may be used to design a feed forward controller in order to eliminate the periodic part of the torque output.

4.5.1 Finding the relationship between frequency and velocity

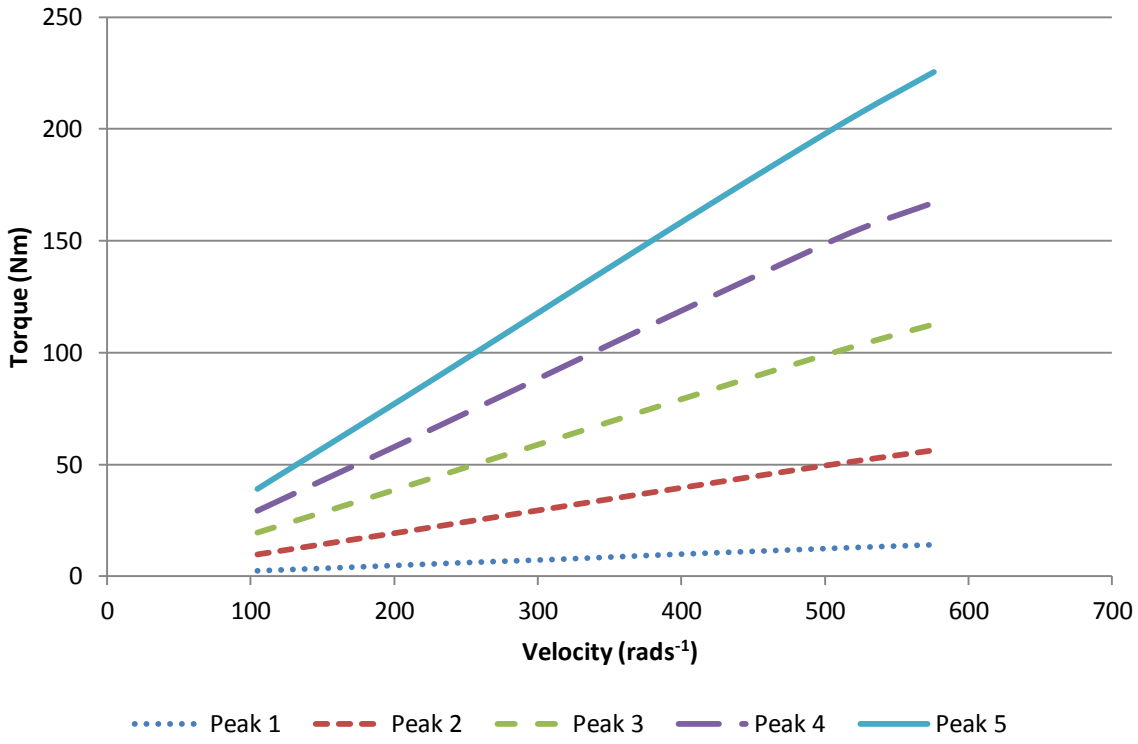

Figure 4.13: Relationship between frequency and velocity

Using the results from the Fourier Transforms, the relationship between the frequency and velocity can be found. As can be seen from Figure 4.13, the frequencies of the 5 dominant sine waves are directly proportional to speed at velocities of 100 rads^{-1}.

This trend is true for all values for the orifice setting. In fact, the gradients of the individual five peaks are the same for all orifice settings. The x-intercept for all waves are 0, since there can be not force generated when the rotor is stationary. This is indicative that the frequency of the periodic part of the signal is independent of the orifice size.

Table 4 below is a table of values of the gradients for the 5 dominant sine waves.

Table 4: Gradient values for the 5 waves

	Gradient
Wave 1	0.025
Wave 2	0.01
Wave 3	0.2
Wave 4	0.3
Wave 5	0.4

4.5.2 Finding the relationship between amplitude and velocity

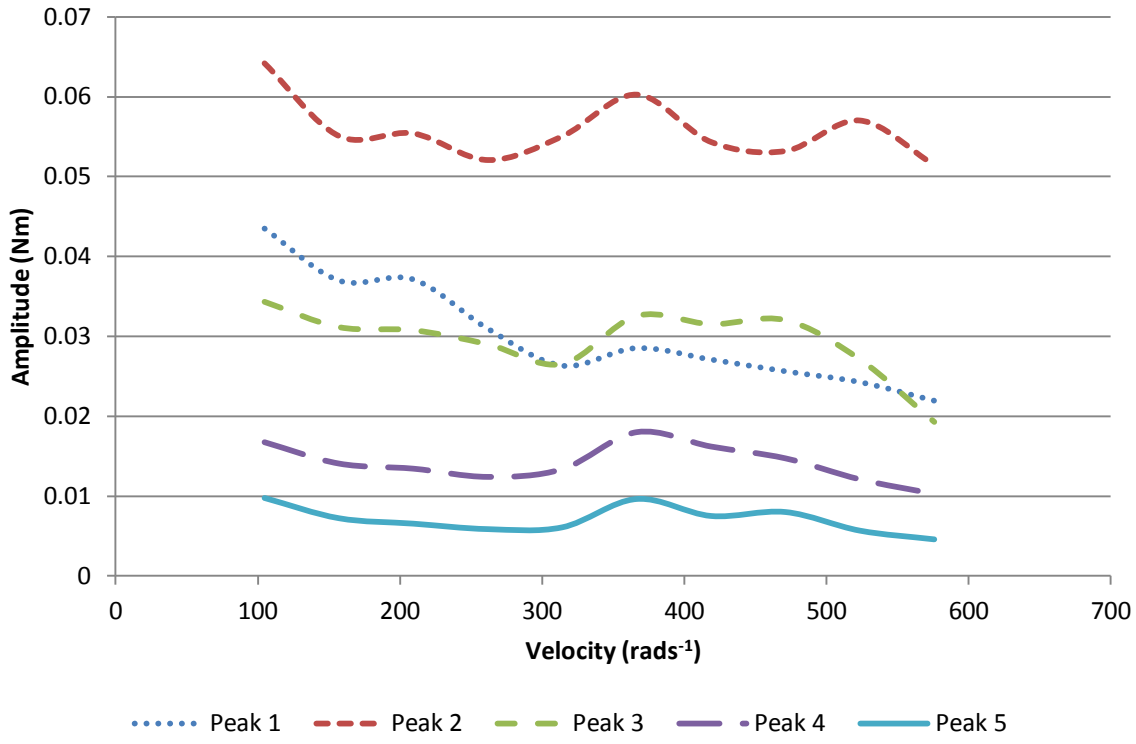

Figure 4.14: Relationship between amplitude and velocity for a 100% open orifice

As with the frequency of the periodic part of the torque output, it is important to understand the relationship between the amplitude of the periodic part and in the input velocity to the damper. Figure 4.14 above is the plot of the amplitude against velocity for an orifice setting of 100% opened. For this particular setting, the amplitude of the 5 waves can be seen from the figure above to decrease with increasing velocity.

While the variation of amplitude against velocity seems to suggest some trend or relationship, this is not as evident for the other orifice settings. For example, Figure 4.15 below shows that the amplitude varies rather erratically with changes in velocity for an orifice setting of 30% opened. This is also true for the test results of the remaining orifice settings.

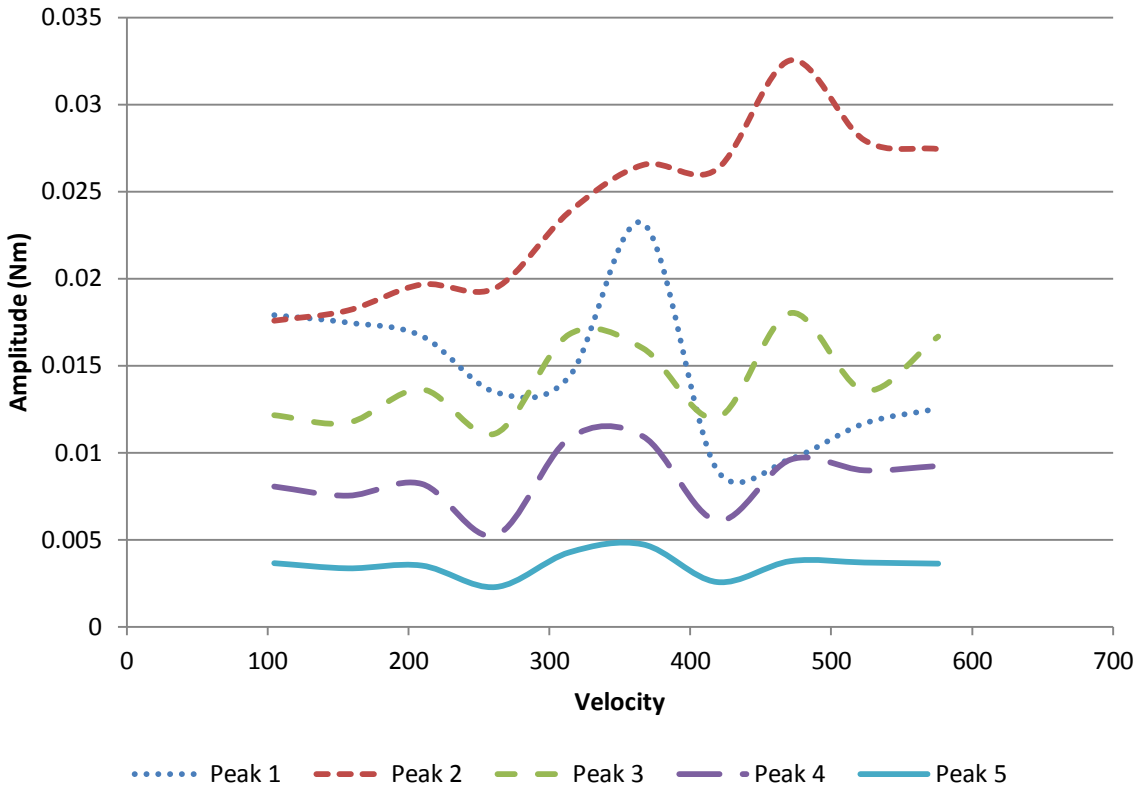

Figure 4.15: Relationship between amplitude and velocity for a 9% open orifice

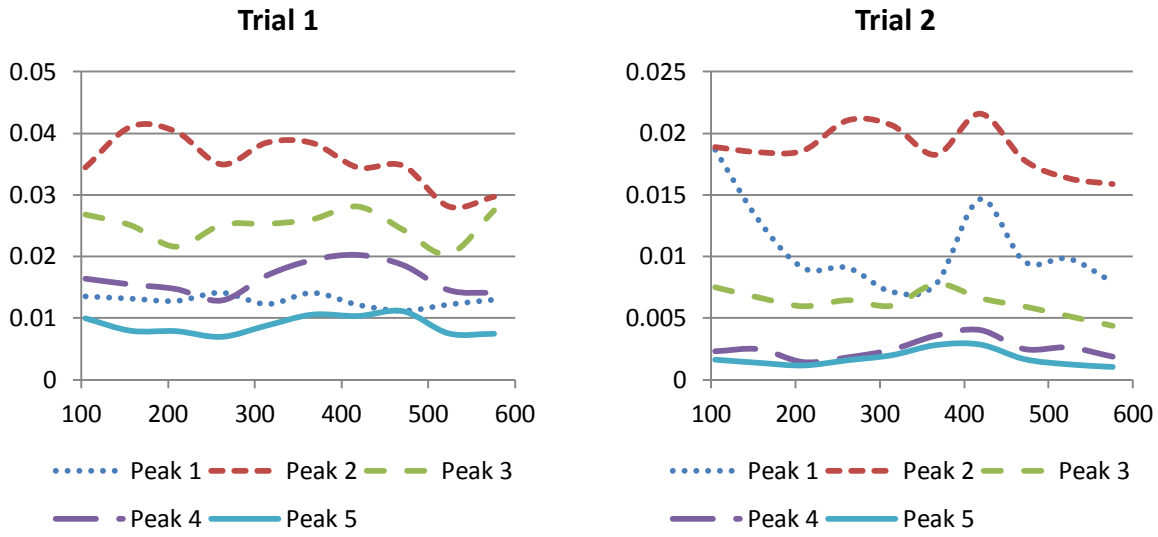

Figure 4.16: Example of 2 trial runs at the same orifice setting of 1% open

Furthermore, it was observed that the amplitude of the dominant waves also vary as the device is run over an extended period of time, or whenever the fluid chamber of the damper is depressurised when the orifice plate is being swapped out.

Figure 4.16 shows two sets of readings that were taken on the same orifice setting. The damper was ran for a complete trial, and then left to rest so as not to overheat the motor. When the second trial was taken, the amplitude of the dominant waves clearly showed a dissimilar pattern as compared to the first.

As such, it can be concluded that the amplitude of the periodic part of the signal does not seem to show a fixed behaviour, particularly if the damper was opened to change the orifice size. An expression to relate the frequency and amplitude of the dominant sine waves to the orifice setting and input velocity was eventually formed; however, it was unable to accurately describe the behaviour of the periodic part of the output signal.

4.6 Assessment of the CRPD design

Much time was invested in the design of the CRPD with the goals of overcoming flaws of the CRVD. After the fabrication of the CRPD, it underwent rigorous testing and subsequently several modifications to improve its performance. However, due to time constraints, the problems encountered in the implementation of the CRPD could not be overcome before the end of the project. The time limitations also prevented the implementation of a controller. Nevertheless, it is still possible to make several assessments on the CRPD.

Low output torque: The main flaw of the CRVD, as pointed out by Alt, is that the output torque is too small for force control to be effective [2]. In fact, the output force of the CRVD was too small to be of any practical use.

One suggested reason for this low output in the CRVD was due to the internal leakage of fluid in the damper. Fluid was able to flow freely over and around the rotor of the damper, bypassing the orifice and therefore reducing the amount of pressure that the damper could build. This reduced the amount of force that the damper could generate.

The CRPD aimed to improve the maximum output torque of the damper by reducing the amount of internal leakage. By using individual piston chambers, the fluid was exposed to the minimum amount of surface area over which the fluid may escape. Moreover, the orifice opening could be more easily controlled.

However, the performance of the CRPD is rather disappointing in that the torque output of the CRPD is not much higher than that of the CRVD. In Alt's

experiments, the CRVD was able to achieve torques of up to 0.25 Nm. In various experiments with the CRPD, the device was able to consistently achieve torques of up to 0.35 Nm, which is only 0.1 Nm more than the CRVD. Considering the output of the CRPD, it is likely that the CRPD would face the same issues as with the CRVD in controller implementation.

However, under certain circumstances, the CRPD was able to produce up to about 1Nm of torque. This usually occurred when excess oil is forced into the piston chamber and the hydraulic oil is more highly pressurised. However, these results were hard to reproduce; separate attempts to highly pressurise the hydraulic fluid produced different torque outputs. This is probably because there is no mechanism to ensure that the pressure in the damper is the same with each refill.

After some time of operation, the high torque output would drop to more consistent levels. This is probably due to some leakages from the mechanical seals used in the interfaces, resulting in a drop of pressure.

One possible reason for the low torque output could be due to the volume flow rate in the damper. Using Equation 3.23 for the cam profile, the flow rate in each piston is given by the following expression:

$$Q_{piston} = 1.13 \times 10^{-6} \omega_{rotor}$$

It can be seen that the volume flow rate of the fluid in the damper rotor is very small. This is due to the cross sectional area of the piston head being made smaller in order to keep the over size of the damper within certain desirable limits.

Considering that the sealing in the rotor is not perfect and some internal leakage will persist, this leakage can be considered significant in comparison to the volume flow rate within the damper.

There are 2 possible ways to remedy this: 1, increase the area of the piston head; or 2, increase the size of the cam to increase the volume of the compression stroke. Both alternatives will however increase the dimensions of the damper. Alternatively, a better variable orifice could be designed to further reduce the internal leakage. For very high force application, the damper could be made to have non-variable orifice to eliminate internal leakages completely.

Variable damping: The CRPD was able to show that controlling the cross-sectional area of an orifice would allow some control over the torque output of the damper. In the identification of the parameters for the non-periodic part of the output signal, an expression relating the damping coefficient (gradient of the curve) to the orifice was found.

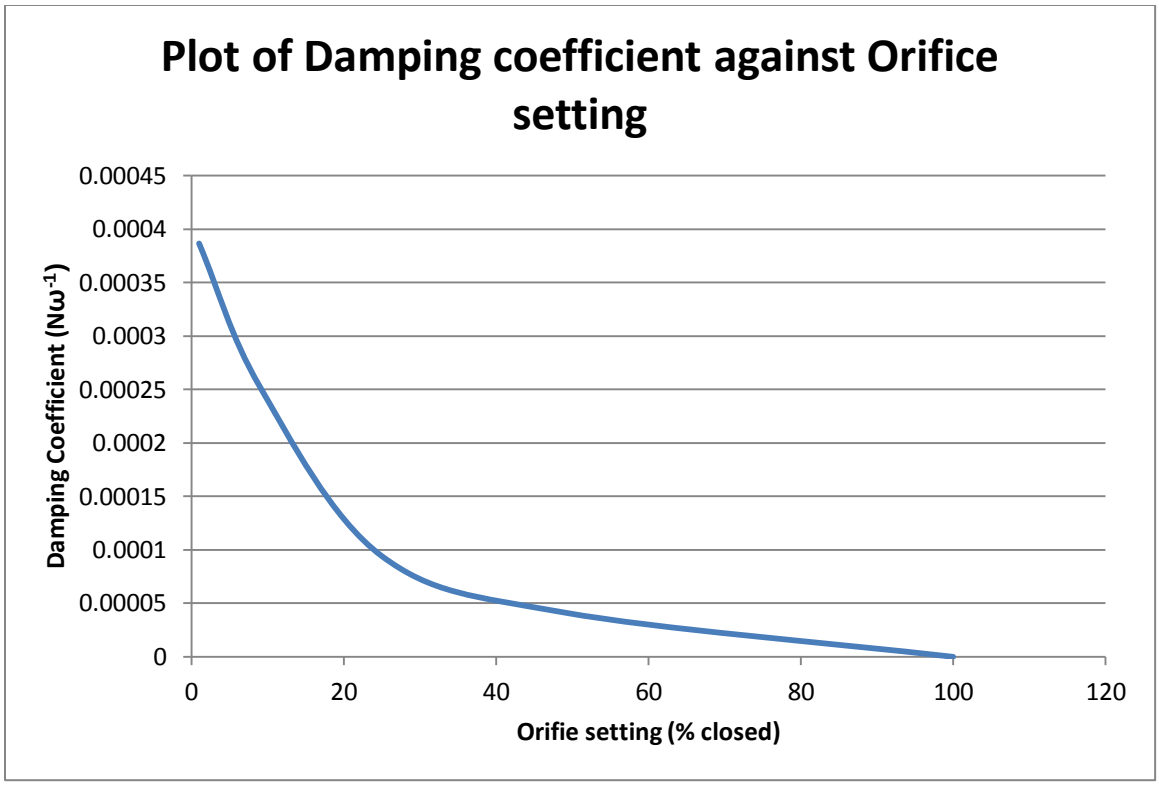

Figure 4.17: Relationship between the damping coefficient and orifice setting

Based on the plot in Figure 4.17, it can be seen that decreasing the cross-sectional area of the orifice opening results in the damping coefficient increasing. This suggests that control of the output torque may be possible through the control of the orifice opening. Considering that the stiction and coulomb friction at low velocities are significant, using the damping coefficient may be a better alternative to achieve precise force control at low torques. More work however, would be needed to further verify this.

Another point where the CRPD succeeds is when the orifice is completely sealed; the rotor of the damper will jam in the stator, allowing for complete torque transmission from the input to the output of the damper. This is ideal as it allows the SDA force actuator to revert from force control to tradition position/velocity

control easily. However, it should be noted that the seals of the damper has a rated loading, and high force will cause the damper to eventually ‘slip’. This limit should be a consideration when designing such damper in the future.

Output signal: In the CRVD, due to the presence of periodic parts in the output signal, Alt had to implement a controller that could compensate for these periodic parts. These periodic parts were due to the mechanical interaction and resulting friction between the rotor, stator, vanes and cam.

In the CRPD, added precautionary measures (e.g. such as roller cam followers, piston guide strips and roller/needle bearings) were taken to further reduce the friction in the damper. The cam of the damper was also designed specifically to eliminate fluctuations in the torque output.

However, due to the highly mechanical nature of the CRPD, the friction in the system introduced significant noise to the output torque of the damper. Moreover, the behaviour of the periodic part of the signal proved to be rather unpredictable.

One reason for this could be due to the internal pressure of the system. When the rotor is opened to either change the orifice setting or hydraulic oil, the pressure in the system changes. This may have caused different torques outputs from the damper, even when the same orifice setting was used.

Furthermore, as the pressure in the system was not really a consideration in the beginning apart from that 1) it should not pass the seal limits and 2) there should be no air in the system, there were no measures taken to ensure a consistent internal pressure at all times. Since the cam system relies on internal pressure to

ensure that the cam followers are in constant contact with the cam wall, the cam followers would lose contact with the cam if there was a loss of pressure due to external leakage. This would lead to cross-over shock.

As the damper was designed to be a self-contained system, such output ‘noise’ is to be expected. It may be possible to reduce the noise due to cross-over shock by highly pressurizing the hydraulic fluid, although more experiments will have to be done to validate this. However, it should be noted that since the design objective was to develop a compact and self-contained solution, it may not be realistic to incorporate any form of pressure maintenance without compromising the size and form factor.

Another possible reason for the unpredictable output signal could be due to the mechanical wear of the components. It was noted after every trial, significant amount of material from the cam wall and piston chamber would be worn away. This high rate of wear is due to the rotor and stator (cum cam) being made of aluminium, while the pistons and cam followers being made of much harder stainless steel to prevent flexing of the piston. Increasing wear on the cam wall could have resulted in the changing behaviour of the amplitude of the periodic part of the signal.

In the initial design phase, it was noted that the material choice may be an issue. However, due to cost constraints and for ease of fabrication, aluminium was chosen. However, future iterations could take this into consideration during the design phase.

In summary, the CRPD was successful in showing that by controlling the cross-sectional area of the orifice; some control over the output torque can be affected. However, the amount of torque produced by the damper was not up to expectations. The design of the orifice section will therefore be very critical in ensuring that minimal internal leakage occurs. Alternatively, the parameters of the damper should be made such that the volume flow rate of the damper fluid is high enough to achieve the desired damping force. However, this will be a trade-off against the size, weight and form factor of the damper.

One area where improvement will prove very challenging is regulating the pressure of the damping fluid in the damper. As the system is a self-contained hydraulic system, it would be very difficult to maintain a constant pressure in the damper, especially when factoring in any external leakages. It would also be necessary to test how long the damper can operate without need to refill and depressurise the system.

Chapter 5 - Conclusion

5.1 Summary

This thesis has presented work done to design a continuous rotary damper for use in the implementation of the Series Damper Actuator (SDA).

Firstly, a quick overview of the state of robotics, as well as the motivation for this project was given. While the SDA was previously successfully implemented using a Magneto-Rheological (MR) fluid damper, the bandwidth of the SDA was limited due to the extra dynamics of the MR damper. The challenge was therefore to design a continuous rotary viscous damper with close to ideal damping properties.

A deeper dive into the various existing forms of force control was then provided to give better insight into the current state of the art. Force criteria such as sufficient bandwidth, low output impedance and high force/torque density was then shared to highlight the strengths and weaknesses of the various forms of force control. A closer look was then taken at the properties and advantages SDA in order to validate the need to design a damper specific for SDA implementation.

A detailed overview was then taken at existing dampers in order to draw inspiration for new novel damper design. The first damper developed was based on the continuous rotary vane damper designed by Chang. By closely examining Chang's design and trying to understand his design reasoning, an improved damper was designed.

The modified continuous rotary damper was tested and analysed in Alt's work, and he was able to implement a controller to compensate for fluctuations in the damper torque

output. However, he noted that the damper output was very low, which limited the effectiveness of the controller.

As the damper output is dependent on the amount of pressure that is generated in the damper fluid, it is critical that as little pressure is lost in the system. However, as the damper fluid is exposed to large interfacing surfaces between the rotor and stator, internal leakages occurred through these gaps, resulting in a loss of pressure and a low force output.

To overcome the shortcomings of the modified continuous rotary vane damper, another novel damper design was proposed based on the radial piston pump design. The design reduced the amount of interfacing surfaces that the fluid was exposed to, hence reducing the amount of internal leakages. However, due to the size parameters of the damper, the resultant volume flow rate in the damper was very small. Although the leakage was reduce, it was still significant compared to the overall flow rate of the hydraulic fluid. As a result, the torque produced by the piston damper was also low, though marginally higher than that of the vane damper.

Also, as the damper design had more mechanical parts than the vane damper, it experienced more friction, increasing its output impedance. The piston damper was also more susceptible to pressure fluctuations in the damper, though little can be done to remedy that since the damper is designed to be a self-contained system. All these resulted in unpredictable fluctuations in the torque output, which would severely limit the implementation of Alt's controller to compensate for these fluctuations.

The piston damper demonstrated that it could achieve variable damping, and was able to achieve one-for-one input to output torque when its orifice is completely sealed. The output torque of the damper was also proportional to input velocity at higher input velocities. Several reasons were suggested for the shortcomings of the damper, and some suggestions were offered as to how to improve on the damper design.

5.2 Future work

In the assessment of the continuous rotary piston damper, it was concluded that further improvement could be done to the design; namely, increasing the torque output of the piston damper.

When compared to the vane damper on a single orifice setting, it can be seen that the two dampers are very similar. As such, it should be possible to implement Alt's controller if the periodic part of the output can be characterised successfully.

Future work would therefore include a redesign of the variable orifice so that the orifice opening can be adjusted without releasing the pressure of the hydraulic fluid. The design parameters could also be revised to increase the volume flow rate of the damper fluid in the rotor to achieve more damping effect. Finally, design optimisations could be done to further reduce the friction in the system.

Should the design improvements be successful, the final stage would be to derive a suitable model that could take the input velocity and orifice size as inputs, with force as the single output. Using Alt's work would be a good basis for the controller implementation.

References

1. Chang, J.S., *Design of Rotary Damper with Varying Damping Effect*, in *Department of Mechanical Engineering*2005, National University of Singapore: Singapore.
2. Alt, S., *System Identication and Control of a Force Control Actuator*, 2012.
3. Kuntze, H.B., et al. *On the application of a new method for fast and robust position control of industrial robots*. in *Robotics and Automation, 1988. Proceedings., 1988 IEEE International Conference on*. 1988.
4. Kazanzides, P., N.S. Bradley, and W.A. Wolovich. *Dual-drive force/velocity control: implementation and experimental results*. in *Robotics and Automation, 1989. Proceedings., 1989 IEEE International Conference on*. 1989.
5. Cetinkunt, S. and S. Wu. *Tip position control of a flexible one arm robot with predictive adaptive output feedback implemented with lattice filter parameter identifier*. in *Robotics and Automation, 1990. Proceedings., 1990 IEEE International Conference on*. 1990.
6. Shin, D.H., D.H. Han, and H.J. Kim. *Open-loop velocity control of the troweling robot*. in *Intelligent Robots and Systems, 1999. IROS '99. Proceedings. 1999 IEEE/RSJ International Conference on*. 1999.
7. Mandal, N. and S. Payandeh. *Force control strategies for compliant and stiff contact: an experimental study*. in *Systems, Man, and Cybernetics, 1994. 'Humans, Information and Technology'., 1994 IEEE International Conference on*. 1994.
8. Eppinger, S.D. and W.P. Seering, *Three dynamic problems in robot force control.* Robotics and Automation, IEEE Transactions on, 1992. **8**(6): p. 751-758.
9. Antonelli, G., N. Sarkar, and S. Chiaverini. *External force control for underwater vehicle-manipulator systems*. in *Decision and Control, 1999. Proceedings of the 38th IEEE Conference on*. 1999.
10. Nemec, B. and L. Zlajpah, *Force control of redundant robots in unstructured environment.* Industrial Electronics, IEEE Transactions on, 2002. **49**(1): p. 233-240.
11. Roy, J. and L.L. Whitcomb. *Adaptive force control of position/velocity controlled robots: theory and experiment*. in *Intelligent Robots and Systems, 2001. Proceedings. 2001 IEEE/RSJ International Conference on*. 2001.
12. Abidi, K., A. Sabanovic, and S. Yesilyurt. *Sliding-mode based force control of a piezoelectric actuator*. in *Mechatronics, 2004. ICM '04. Proceedings of the IEEE International Conference on*. 2004.
13. Sun, H. and G.T.C. Chiu. *Nonlinear observer based force control of electro-hydraulic actuators*. in *American Control Conference, 1999. Proceedings of the 1999*. 1999.
14. Pratt, G.A., et al., *Stiffness Isn't Everything*, in *The 4th International Symposium on Experimental Robotics IV*1997, Springer-Verlag. p. 253-262.
15. Xu, Y. and R.P. Paul. *On position compensation and force control stability of a robot with a compliant wrist*. in *Robotics and Automation, 1988. Proceedings., 1988 IEEE International Conference on*. 1988.

16. Youcef-Toumi, K. and D.A. Gutz. *Impact and force control*. in *Robotics and Automation, 1989. Proceedings., 1989 IEEE International Conference on*. 1989.
17. Sugano, S., S. Tsuto, and I. Kato. *Force Control Of The Robot Finger Joint Equipped With Mechanical Compliance Adjuster*. in *Intelligent Robots and Systems, 1992., Proceedings of the 1992 lEEE/RSJ International Conference on*. 1992.
18. Vischer, D. and O. Khatib, *Design and development of high-performance torque-controlled joints.* Robotics and Automation, IEEE Transactions on, 1995. **11**(4): p. 537-544.
19. Pratt, G.A. and M.M. Williamson. *Series elastic actuators*. in *Intelligent Robots and Systems 95. 'Human Robot Interaction and Cooperative Robots', Proceedings. 1995 IEEE/RSJ International Conference on*. 1995.
20. Williamson, M.M., *Series elastic actuators*, 1995, Massachusetts Institute of Technology. p. 80 p.
21. Robinson, D.W., et al. *Series elastic actuator development for a biomimetic walking robot*. in *Advanced Intelligent Mechatronics, 1999. Proceedings. 1999 IEEE/ASME International Conference on*. 1999.
22. Sulzer, J.S., M.A. Peshkin, and J.L. Patton. *MAMONET: An exotendon-driven rotary series elastic actuator for exerting joint torque*. in *Rehabilitation Robotics, 2005. ICORR 2005. 9th International Conference on*. 2005.
23. Sensinger, J.W. and R.F.f. Weir. *Design and analysis of a non-backdrivable series elastic actuator*. in *Rehabilitation Robotics, 2005. ICORR 2005. 9th International Conference on*. 2005.
24. Chew, C.M., G.S. Hong, and W. Zhou. *Series damper actuator: a novel force/torque control actuator*. in *Humanoid Robots, 2004 4th IEEE/RAS International Conference on*. 2004.
25. Zhou, W., *Analysis and Synthesis of Series Damper Actuator*, in *Department of Mechanical Engineering, Control & Mechatronics*2002, National Univeristy of Singapore: Singapore.
26. Zhou, W., C.M. Chew, and G.S. Hong. *Property analysis for series MR-fluid actuator system*. in *Robotics, Automation and Mechatronics, 2004 IEEE Conference on*. 2004.
27. Whitney, D.E. *Historical perspective and state of the art in robot force control*. in *Robotics and Automation. Proceedings. 1985 IEEE International Conference on*. 1985.
28. Yoshikawa, T. *Force control of robot manipulators*. in *Robotics and Automation, 2000. Proceedings. ICRA '00. IEEE International Conference on*. 2000.
29. Gorinevsky, D.M., A.M. Formalsky, and A.Y. Schneider, *Force Control of Robotic Systems*, 1998, CRC-Press. p. 368.
30. Salisbury, J.K. *Active stiffness control of a manipulator in cartesian coordinates*. in *Decision and Control including the Symposium on Adaptive Processes, 1980 19th IEEE Conference on*. 1980.
31. Qian, H.P. and J. De Schutter. *Introducing active linear and nonlinear damping to enable stable high gain force control in case of stiff contact*. in *Robotics and Automation, 1992. Proceedings., 1992 IEEE International Conference on*. 1992.

32. Whitney, D.E., *Force Feedback Control of Manipulator Fine Motions.* Journal of Dynamic Systems, Measurement, and Control, 1977. **99**(2): p. 91-97.
33. Hogan, N., *Impedance Control: An Approach to Manipulation: Part I---Theory.* J. Dyn. Sys., Meas., Control, 1985. **107**(1): p. 7.
34. Neville, H., *Impedance Control: An Approach to Manipulation: Part I---Theory.* Journal of Dynamic Systems, Measurement, and Control, 1985. **107**(1).
35. Jung, S., T.C. Hsia, and R.G. Bonitz, *Force tracking impedance control of robot manipulators under unknown environment.* Control Systems Technology, IEEE Transactions on, 2004. **12**(3): p. 474-483.
36. Seraji, H.O. *Adaptive admittance control: an approach to explicit force control in compliant motion*. in *Robotics and Automation, 1994. Proceedings., 1994 IEEE International Conference on*. 1994.
37. Mason, M.T., *Compliance and Force Control for Computer Controlled Manipulators.* Systems, Man and Cybernetics, IEEE Transactions on, 1981. **11**(6): p. 418-432.
38. Anderson, R.J. and M.W. Spong, *Hybrid impedance control of robotic manipulators.* Robotics and Automation, IEEE Journal of, 1988. **4**(5): p. 549-556.
39. Volpe, R. and P. Khosla, *A theoretical and experimental investigation of explicit force control strategies for manipulators.* Automatic Control, IEEE Transactions on, 1993. **38**(11): p. 1634-1650.
40. Zeng, G. and A. Hemami, *An overview of robot force control.* Robotica, 1997. **15**(05): p. 473-482
41. Fauteux, P., et al. *Dual differential rheological actuator for robotic interaction tasks*. in *Advanced Intelligent Mechatronics, 2009. AIM 2009. IEEE/ASME International Conference on*. 2009.
42. Zinn, M., et al., *Actuation Methods For Human-Centered Robotics and Associated Control Challenges*, in *Control Problems in Robotics*2003, Springer Berlin / Heidelberg. p. 105-120-120.
43. Kaminaga, H., et al. *Backdrivability analysis of Electro-Hydrostatic Actuator and series dissipative actuation model*. in *Robotics and Automation (ICRA), 2010 IEEE International Conference on*. 2010.
44. Yabuta, T., et al., *Force control of servomechanism using adaptive control.* Robotics and Automation, IEEE Journal of, 1988. **4**(2): p. 223-228.
45. Wilfinger, L.S., J.T. Wen, and S.H. Murphy, *Integral force control with robustness enhancement.* Control Systems, IEEE, 1994. **14**(1): p. 31-40.
46. Whitcomb, L.L., et al., *Experiments in adaptive model-based force control.* Control Systems, IEEE, 1996. **16**(1): p. 49-57.
47. Cortesao, R., et al. *Explicit force control for manipulators with active observers*. in *Intelligent Robots and Systems, 2000. (IROS 2000). Proceedings. 2000 IEEE/RSJ International Conference on*. 2000.
48. Gevarter, W.B., *Basic relations for control of flexible vehicles.* AIAA Journal 1970. **8**(4).
49. Colgate, E. and N. Hogan. *An analysis of contact instability in terms of passive physical equivalents*. in *Robotics and Automation, 1989. Proceedings., 1989 IEEE International Conference on*. 1989.

50. Asada, H., T. Kanade, and I. Takeyama, *Control of a Direct-Drive Arm.* J. Dyn. Sys., Meas., Control, 1983. **105**(3).
51. Aghili, F., M. Buehler, and J.M. Hollerbach. *Development of a high performance direct-drive joint*. in *Intelligent Robots and Systems, 2000. (IROS 2000). Proceedings. 2000 IEEE/RSJ International Conference on*. 2000.
52. Tonietti, G., R. Schiavi, and A. Bicchi. *Design and Control of a Variable Stiffness Actuator for Safe and Fast Physical Human/Robot Interaction*. in *Robotics and Automation, 2005. ICRA 2005. Proceedings of the 2005 IEEE International Conference on*. 2005.
53. Schiavi, R., et al. *VSA-II: a novel prototype of variable stiffness actuator for safe and performing robots interacting with humans*. in *Robotics and Automation, 2008. ICRA 2008. IEEE International Conference on*. 2008.
54. Wolf, S. and G. Hirzinger. *A new variable stiffness design: Matching requirements of the next robot generation*. in *Robotics and Automation, 2008. ICRA 2008. IEEE International Conference on*. 2008.
55. Morrell, J.B. and J.K. Salisbury. *Parallel coupled actuators for high performance force control: a micro-macro concept*. in *Intelligent Robots and Systems 95. 'Human Robot Interaction and Cooperative Robots', Proceedings. 1995 IEEE/RSJ International Conference on*. 1995.
56. Zinn, M., O. Khatib, and B. Roth. *A new actuation approach for human friendly robot design*. in *Robotics and Automation, 2004. Proceedings. ICRA '04. 2004 IEEE International Conference on*. 2004.
57. de Silva, C.W., *Introduction*, in *Vibration Damping, Control, and Design*, C.W.d. Silva, Editor 2007, CRC Press: Boca Raton. p. 1-8.
58. Norton, R.L., *Cam Design*, in *Design of Machinery: An introduction to the Synthesis and Analysis of Meachanisms and Machines*1999, McGraw-Hill series in mechanical engineering.
59. Flitney, R.K., *Static seals*, in *Seals and sealing handbook*2007, Butterworth-Heinemann.
60. *Engineered Surfaces in Hydrostatic Applications*. [cited 2011 25th June]; Available from: http://www.timken.com/en-us/products/coatings/engineered/Pages/ESinHydrostaticApplications.aspx.
61. *Hitech Seals Inc.*; Available from: http://www.hitechseals.com/index.asp?lang=.
62. Alt, S., *System Identication and Control of a Force Control Actuator*, 2012, National University of Singapore. p. 39 - 40.
63. ATI Industrial Automation, I., in *Photoshop*, M.-E. low_res.jpg, Editor 2012, ATI Industrial Automation, Inc.: http://www.ati-ia.com/app_content/product_images/Mini45-E%20low_res.jpg.